AD-A070 808 NATIONAL BUREAU OF STANDARDS WASHINGTON DC POLYMER --ETC F/G 20/3
PIEZO AND PYROELECTRIC PROPERTIES OF ELECTRETS.(U)
JUN 79 M G BROADHURST, G T DAVIS N00014-79-C-0012
UNCLASSIFIED TR-10 NL

| OF |
AD
A070 808

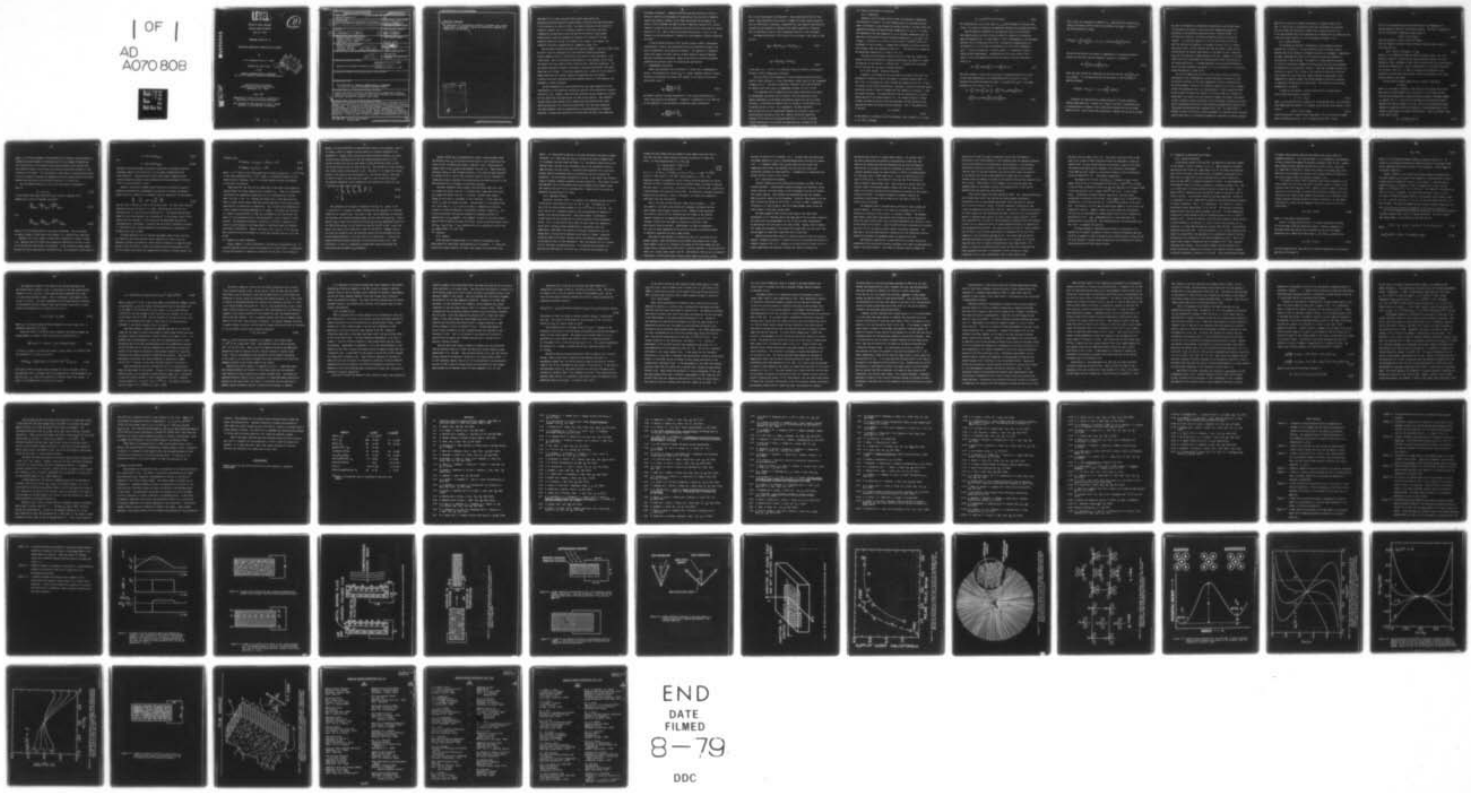

END
DATE
FILMED
8-79
DDC

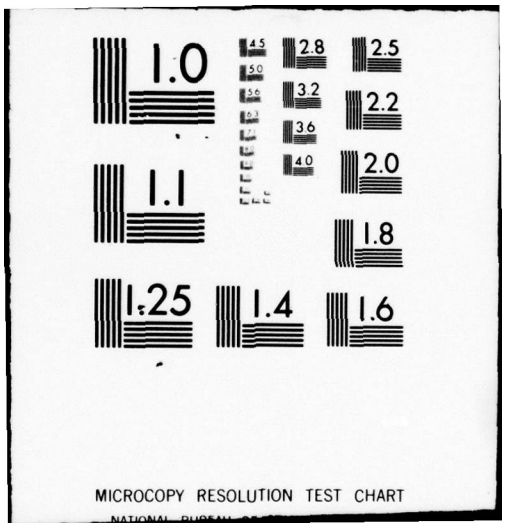
1.0
1.1
1.25
1.4
1.6
1.8
2.0
2.2
2.5
2.8
3.2
3.6
4.0
4.5
5.0
5.6
6.3
MICROCOPY RESOLUTION TEST CHART

OFFICE OF NAVAL RESEARCH

Contract N0014-79-C-0012

Task No. 12139

TECHNICAL REPORT NO. 10

PIEZO AND PYROELECTRIC PROPERTIES OF ELECTRETS

by

M. G. Broadhurst and G. T. Davis

Prepared for Publication

in the

Topics in Modern Physics - Electrets
Ed, by G. M. Sessler, Published by Springer-Verlag

National Bureau of Standards
Polymer Science & Standards Division
Washington, D.C. 20234

June, 1979

SECURITY CLASSIFICATION OF THIS PAGE (When Data Entered)

REPORT DOCUMENTATION PAGE

READ INSTRUCTIONS BEFORE COMPLETING FORM

1. REPORT NUMBER: Technical Report # 10	2. GOVT ACCESSION NO.
3. RECIPIENT'S CATALOG NUMBER: (9)	
4. TITLE (and Subtitle): (6) PIEZO AND PYROELECTRIC PROPERTIES OF ELECTRETS.	5. TYPE OF REPORT & PERIOD COVERED: Technical Report # 10 (13)
	6. PERFORMING ORG. REPORT NUMBER
7. AUTHOR(s): (10) M. G. Broadhurst G. T. Davis	8. CONTRACT OR GRANT NUMBER(s): (15) N00014-79-C-0012
9. PERFORMING ORGANIZATION NAME AND ADDRESS: National Bureau of Standards, Polymer Science & Standards Division, Washington, D.C. 20234	10. PROGRAM ELEMENT, PROJECT, TASK AREA & WORK UNIT NUMBERS: Task No. 12139
11. CONTROLLING OFFICE NAME AND ADDRESS: Office of Naval Research, Chemistry Program, Arlington, VA 22217 (14) TR-10	12. REPORT DATE: (11) Jun[redacted]79
	13. NUMBER OF PAGES: 52
14. MONITORING AGENCY NAME & ADDRESS (if different from Controlling Office): (12) 74 p.	15. SECURITY CLASS. (of this report): Unclassified
	15a. DECLASSIFICATION/DOWNGRADING SCHEDULE

16. DISTRIBUTION STATEMENT (of this Report)

According to attached distribution list.

This document has been approved for public release and sale; its distribution is unlimited.

17. DISTRIBUTION STATEMENT (of the abstract entered in Block 20, if different from Report)

18. SUPPLEMENTARY NOTES

To be published in "Topics in Modern Physics - Electrets"
Ed. by G. M. Sessler, published by Springer-Verlag

19. KEY WORDS (Continue on reverse side if necessary and identify by block number)

Crystal relaxations; electrets; ferroelectricity; piezoelectric polymers; polarization; poly(vinyl chloride); poly (vinyl fluoride); poly (vinylidene fluoride); pyroelectric polymers; space charge.

20. ABSTRACT (Continue on reverse side if necessary and identify by block number)

Electrets with piezoelectric and pyroelectric properties can be made from thin polymer films which have the desirable properties of being flexible, strong, and light weight. The properties of electrets composed or oriented molecular dipoles in both amorphous and semicrystalline polymers are compared with monopolar electrets formed by frozen-in real charge. Models and concepts are presented which allow piezoelectric and pyroelectric response to be predicted from materia properties. A two-site model of dipole alignment involving cooperativity leads

Next page

DD FORM 1 JAN 73 1473 EDITION OF 1 NOV 65 IS OBSOLETE
S/N 0102-014-6601

SECURITY CLASSIFICATION OF THIS PAGE (When Data Entered)

Block 20 - continued

to predictions for ferroelectric switching in polymers with a polar crystal form. Experimental results are reviewed and compared with predictions from the model.

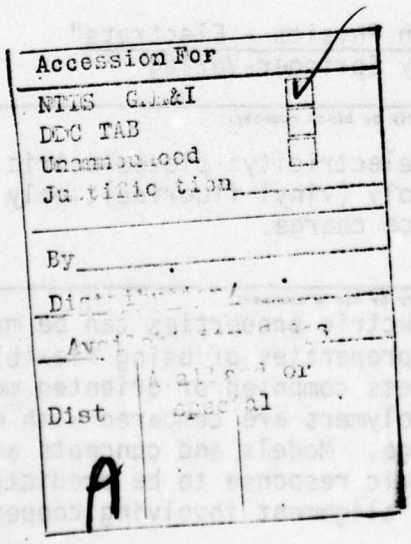

HEAVISIDE [4.1] in 1892, postulated that certain waxes would form permanently polarized dielectrics when allowed to solidify from the molten state in the presence of an electric field. He viewed an electret as the electrical analog of a magnet, that is, as having a frozen-in, relatively long lived (compared to the observation time) non-equilibrium electric dipole moment. Present popular usage has expanded this concept of an electret to include monopolar dielectrics having a net frozen-in real charge. For example, the commercial electret microphone employs a monopolar polymer film.

Wax and rosin electrets were made and studied by EGUCHI in the early 1920's [4.2]. By 1927 it was well understood [4.3] that molecules containing permanent electric moments orient in the direction of an electric field when mobile in the liquid state. Upon solidification of the material in the presence of the field, the dipoles lose their mobility while retaining their preferred orientation. The net dipole orientation produces the electret's permanent polarization (net dipole moment per unit volume). It was also recognized that in addition to the electret's moment there were real charges, generally concentrated near the electret surfaces, which were injected during the formation process by field emission, gas breakdown or similar processes.

In 1927 piezoelectricity and pyroelectricity were shown theoretically and experimentally to be properties exhibited by electrets with preferentially ordered dipoles [4.3, 4]. However, these early wax electrets had poor mechanical strength and low sensitivity, and applications for them did not develop. More recently, strong, highly active polymer films, notably poly(vinylidenefluoride), PVDF, poly(vinylfluoride), PVF, and poly(vinylchloride), PVC, have been recognized for their potential value as thermolelectric and electromechanical transducer materials. Already these materials are finding their way into a new technology

of polymer transducers. Japanese scientists have been particularly active in the early research and development of these devices with the work of FUKADA on natural and synthetic polymers [4.5], KAWAI who pointed out how general the effect is [4.6], HAYAKAWA and WADA with their theoretical analyses [4.7, 8] and industrial scientists who are developing films [4.9,10] and using them for various devices [4.11-13]. Most of the early polymer electret work in the U. S. has focused on using the pyroelectric response for electromagnetic radiation detection [4.14-22].

In the following sections we shall present concepts, models, experimental considerations, results, and implications which have resulted from some of the work on piezoelectric and pyroelectric polymers. This approach is intended to provide the reader with basic physical concepts needed to identify important molecular and material parameters, deduce guide-lines for optimizing desirable properties and provide a basis for selecting new applications.

4.1 Thermodynamic Definitions

Piezo- and pyroelectricity are defined in a formal way by thermodynamics [4.23]. The piezoelectric constant d_{mj}, is a tensor component given by a second derivative of the Gibbs free energy with respect to the electric field vector $\underline{E}$ and stress tensor T.

$$d_{mj} = \left[\frac{\partial^2 G(\underline{E}, \underline{T}, T)}{\partial E_m \partial T_j}\right]_T \tag{4.1}$$

We define a material as being piezoelectric if this second derivative has a value large enough to be measurable. A material is pyroelectric if at least one of the components of the pyroelectric coefficient vector $\underline{p}$ defined as

$$p_m = \left[\frac{\partial^2 G(\underline{E}, \underline{T}, T)}{\partial E_m \partial T}\right]_{\underline{T}} \tag{4.2}$$

has a value large enough to be measurable. Being second derivatives of free energy, these coefficients have a basis in common with better known quantities such as coefficients of expansion, compressibility, heat capacity and dielectric constant and can therefore be expected to be complex quantities if measured with an alternating stress or show relaxational behavior in the time domain.

The second derivatives in (4.1) and (4.2) can be taken in any order so that we have,

$$d_{mj} = (\partial D_m/\partial T_j)_{T,\underline{E}} = (\partial S_j/\partial E_m)_{\underline{T},\ T} \qquad (4.3)$$

and

$$p_m = (\partial D_m/\partial T)_{\underline{E}} = (\partial \Sigma/\partial E_m)_T \qquad (4.4)$$

In the above, j=1,...6; m=1, 2, 3; $\underline{T}$=stress; S=strain; D=electric displacement; E=electric field; T=temperature; Σ=entropy.

The d are often called piezoelectric strain constants whereas the piezoelectric stress constants, e, arise from taking S rather than $\underline{T}$ as the independent variable in (4.1). Two other piezoelectric constants h and g can be defined by taking D and S and D and $\underline{T}$ as independent variables in (4.1), [4.24].

It is important here to emphasize that the above relationships are based on thermodynamic quantities such as electric field and mechanical stress, whereas experiments are performed using measured quantities such as voltage and force. A derivative at constant force or voltage is not the same as one at constant stress or field. As a consequence, the above equations must be used with care for experimental purposes as discussed in Sec 4.2.3, and pointed out previously [4.25, 26]. Before relating the quantities defined in (4.3) and (4.4) to measured quantities, it is well to develop a better description of an electret and understand the influence of real and dipolar charges.

4.2 Physical Description of an Electret

4.2.1 Preparation

Consider a slab of polymer which we take to be amorphous, homogeneous, and elastically isotropic. We first evaporate metallic electrodes on both sides to eliminate air gaps between the polymer and metal, and then follow the temperature-voltage-time sequence shown schematically in Fig. 4.1: 1) raise the temperature from room temperature T_r to an elevated temperature which we show here as being above the glass transition temperature, T_g; 2) apply a dc voltage, Φ, resulting in an electric field of several hundred kilovolts per centimeter of slab thickness, s, between the electrodes; 3) while maintaining this voltage, lower the temperature back to T_r . The electret thus formed can be represented schematically as shown in Fig. 4.2.

The above poling procedure typically results in both real charges and charges resulting from molecular dipoled distributions, and these will affect the behavior of the electret in different ways. To explain this difference we will consider the two types of charge separately.

4.2.2 Real Charges - Monopolar Electrets

In general, real charges do not contribute to the zero field piezo- and pyroelectric response as long as the sample is strained uniformly [Ref. 4.7, Sec. 2.2]. To illustrate this fact, consider the example of Fig. 4.3. A slab of dielectric with uniform permittivity ε thickness s and short circuited contact electrodes contains a layer of trapped positive charges at a distance, x, from the bottom electrode. The charge density on the top electrode is σ_s and the charge density of the trapped charge is σ_x. The trapped charge will induce an equal and opposite charge on the two electrodes divided according to the capacitance between the charge and the electrodes. Thus if the permittivity is uniform,

$$\sigma_s = -\sigma_x(x/s) \tag{4.5}$$

If the material is strained so that the distances x and s change to $x + \Delta x$ and $s + \Delta s$, then σ_s becomes:

$$\sigma'_s = -\sigma_x (x/s)[(1+\Delta x/x)/(1+\Delta s/s)] \qquad (4.6)$$

For uniform strain, $\Delta x/x = \Delta s/s$. then $\sigma'_s = \sigma_s$ and no charge will flow (at zero field) as a result of pressure and temperature changes which produce the strain.

When the material properties or the resultant strain are non-uniform, the trapped charges can give rise to an electrical response as discussed by Wada and Hayakawa [4.8]. In their model, a film is heterogeneous in the thickness direction only (x direction in Fig. 4.3). The density of space-charge $\rho(x)$ and permittivity $\varepsilon(x)$ are position dependent as are the stress dependences $\alpha_\varepsilon(x) \equiv \partial \ln \varepsilon(x)/\partial X$ and $\alpha_x(x) \equiv \partial \ln x/\partial X$, where X is a mechanical stress or thermal stress (temperature). Considering the film to be a stack of thin layers, (4.5) can be generalized to give the charge on the top electrode of areas A_s as,

$$Q_s = -\int_0^s \rho(x) A_s dx \int_0^x dx'/\varepsilon(x') / \int_0^s dx'/\varepsilon(x') \qquad (4.7)$$

The total charge in a given layer, $\rho(x)\, A_s dx$ is assumed constant with stress. In the linear approximation the strained quantities dx' and $\varepsilon(x')$ can be replaced with unstrained quantities $dx_o[1 + \alpha_x(x_o)dX]$ and $\varepsilon(x_o)[1 + \alpha_\varepsilon(x_o)dX]$. Expanding to first order in the α's,

$$Q_s = -\int_0^s \rho(x) A_s dx \int_0^x dx_o/\varepsilon \left\{1 \quad [\int_0^x \varepsilon^{-1}(\alpha_x - \alpha_\varepsilon) dX dx_o / \int_0^x dx_o/\varepsilon] \right.$$

$$\left. -[\int_0^s \varepsilon^{-1}(\alpha_x - \alpha_\varepsilon) dX dx_o / \int_0^s dx_o/\varepsilon] \right\} / \int_0^s dx_o/\varepsilon \qquad (4.8)$$

The α's and ε are understood to depend on x_o. Subtracting the unstrained Q_{so} from Q_s and assuming uniform stress dX one obtains the change in charge on the top electrode with stress,

$$A^{-1}\partial Q_s/\partial X = -\int_o^s \rho(x)\left\{\int_o^x [(\alpha_x - \alpha_\varepsilon) - <\alpha_x - \alpha_\varepsilon>]dx_o/\varepsilon(x_o)\right\}dx\int_o^s dx_o/\varepsilon(x_o) \qquad (4.9)$$

The partial derivative with respect to temperature is at constant mechanical stress and vice versa, and the average of a quantity is defined as

$$<A> = \int_o^s A dx_o/\varepsilon(x_o) / \int_o^s dx_o/\varepsilon(x_o). \qquad (4.10)$$

Using the usual formula for integration by parts and the fact that $\int_o^s [(\alpha_x - \alpha_\varepsilon) - <\alpha_x - \alpha_\varepsilon>]dx_o/\varepsilon = 0$, the above equation can be written in the form given by Wada and Hayakawa,

$$A^{-1}\partial Q_s/\partial X = <[(\alpha_x - \alpha_\varepsilon) - <\alpha_x - \alpha_\varepsilon>][\int_o^x \rho(x_o)dx_o]> \qquad (4.11)$$

In general the response due to trapped charge will be small because of limited charge densities. Crosnier et al found a low level of piezoelectricity in polypropylene and showed a linear relationship between activity and charge density [4.27]. Ibe has shown that piezoelectric response from non polar polymers

can result from bending a specimen which establishes a non-uniform stress in the material and creates a condition where trapped space charge can contribute to the electrode charge when stress is applied [4.28]. To calculate this effect Eq. (4.9) must be modified leaving dX inside the integral. The resulting equation will be like that used by Collins to describe the electrical response of a charged, non-polar film to a thermal heat pulse [4.29]. Collins used the fact that the thermal stress was non-uniform during the thermal equilibration of the sample to gain information about the distribution of trapped charge in the film. DeReggi et al [4.30] showed that such an experiment can provide several Fourier coefficients of the charge distribution. A related experiment using non-uniform mechanical stress has been proposed by Laurenceau et al as an alternative way of measuring charge distribution in films [4.31].

Eq. (4.11) suggests the possibility that one can create an artificial piezoelectric from a heterogeneous structure designed to optimize $\rho(x)$ and the spatial variations in the stress dependence of strain and permittivity. An obvious example is shown in the schematic diagram of Fig. 4.4 of a charged polymer film mounted so that an air gap separates it from a conductive plate. As the charged film moves with respect to the plate (under the influence of sound waves, for example) the plate potential changes and charges flow between it and a conductive contact electrode on the film through an appropriate circuit. This is the operating principle of the electret microphone which typically uses fluorinated ethylene-proplylene copolymer [4.32, 33]. This same effect is probably a source of electrical signals generated in a flexible polymer-insulated coaxial cable when it is subjected to mechanical vibrations or pressure changes.

Note that the electret microphone system does not undergo *uniform* strain. That is, the air gap is strained much more than the polymer film and hence the real charges do contribute to current flow in accord with Eq (4.11). It has been proposed that such a mechanism may be responsible for piezoelectricity in polyvinylidene fluoride, as will be discussed in Subsect. 4.5.4.

4.2.3 Dipolar Electret

To illustrate the electret's piezoelectric and pyroelectric behavior consider Fig. 4.5 and 4.6. As the electrically short-circuited electret contracts due to an increase in hydrostatic pressure or a decrease in temperature the metal electrodes move closer to the dipoles and the zero potential is maintained by a flow of charge. This model of a strain sensitive electret is similar to that given by ADAMS [4.3] and accounts for most of the response of piezoelectric and pyroelectric polymers. Note that the model predicts the direction of current flow in terms of the direction of the poling field and also predicts that while the total charge released is proportional to the temperature or pressure change, the current depends on the rate of pressure or temperature change and can be quite large. This effect can be described mathematically as follows.

In terms of the material's relative permittivity ε^1 the equilibrium field-induced polarization is given by,

$$P = (\varepsilon^1 - 1)\varepsilon_o E \tag{4.12}$$

where $_o$is the permittivity of vacuum and E is the applied field. At sufficiently high temperatures the material is a dipolar liquid and the field produces a polarization

$$P_L(T) = (\varepsilon_L(T)-1)\varepsilon_o E_p \tag{4.13}$$

where the subscript L refers to the liquid phase, (T) to the functional dependence on temperature and $E_p = \Phi/s$ is the mean poling field. During

poling, the field maintains this polarization while the temperature is lowered enough to immobilize the molecular dipoles. The field is removed and the lost polarization (neglecting volume change) is,

$$P_s(T) = [\varepsilon'_s(T)-1]\varepsilon_o E_p \tag{4.14}$$

where the subscript s refers to the solid phase.

Thus the frozen-in non-equilibrium polarization remaining after removal of the poling field is:

$$P_o(T) = [\varepsilon'_L(T_L)-\varepsilon'_s(T)]\varepsilon_o E_p = \Delta\varepsilon'\varepsilon_o E_p \tag{4.15}$$

where T_L is the temperature where the material becomes liquid. Eq. (4.15) provides a method of calculating the frozen dipole polarization for linear dielectrics from a knowledge of their relative permittivity at the polarization and measuring temperatures. Special consideration of non-linear dielectrics will be given in Sec 4.5. In order to calculate the piezoelectric and pyroelectric coefficients from molecular properties one needs to use a more detailed model as shown below.

The polarization (dipole moment per unit volume) is defined as

$$P = N\langle m\rangle/V \tag{4.16}$$

where N is the number of dipoles, V the volume of the electret and $\langle m\rangle$ the mean effective dipole moment in the direction of P. As a model for the electret with preferentially ordered polarizable dipoles of permanent moment μ_o, consider Fig. 4.7. One can use an Onsager type calculation [4.34] to determine the effective moment $\langle m\rangle$ in Eq. (4.16) of a representative dipole located in a spherical cavity and oriented at a fixed average angle θ with respect to the direction of overall polarization P. Such a calculation leads to the result [4.35]:

$$P_o = (\varepsilon_\infty+2)N\mu_o\langle\cos\theta\rangle/3V \tag{4.17}$$

where ε_∞ is the high frequency relative permittivity related to the polarizability through the Clausius-Mosotti relationship and N/V is the number of dipoles per unit volume and P_o is the frozen-in polarization present at zero applied field. This important equation can be used to calculate the piezo-and pyroelectric coefficients for this model. This calculation is done simply by taking the derivatives of P_o with respect to pressure and temperature and then expressing the relationship between these derivatives and the define quantities (4.3) and (4.4).

The relationship between P_o of Eq. (4.17) and electric displacement is given by

$$D = \varepsilon'\varepsilon_o E + P_o \tag{4.18}$$

In the simplest case where the short-circuit current is measured while temperature or stress are changed, one obtains:

$$\left.\frac{\partial D}{\partial \underline{T}}\right|_{E=0,T} = \left.\frac{\partial P_o}{\partial \underline{T}}\right|_{E=0,T} = \left.\frac{\partial (Q/A)}{\partial \underline{T}}\right|_{E=0,T} \tag{4.19}$$

and

$$\left.\frac{\partial D}{\partial T}\right|_{E=0,\underline{T}} = \left.\frac{\partial P_o}{\partial T}\right|_{E=0,\underline{T}} = \left.\frac{\partial (Q/A)}{\partial T}\right|_{E=0,\underline{T}} \tag{4.20}$$

where Q/A is the surface charge per unit area of electrode. Here we continue to neglect changes in (Q/A) due to real charges, i.e., uniform strain conditions.

Generally it is not a change in (Q/A) which is measured but rather a change in Q. Reported values for piezo- and pyroelectric coefficients are thus in error as far as the strict definitions are concerned. In the following we adopt common practice and define experimentally determined piezo- and pyroelectric coefficients as,

$$d = (1/A)\ (\partial Q/\partial \underline{T})_{E=0,T} \tag{4.21}$$

and

$$p = (1/A)\ (\partial Q/\partial T)_{E=0,\underline{T}} \tag{4.22}$$

The above distinction becomes particularly significant for polymers where the difference between (4.19) and (4.21) is of the order of magnitude of the terms themselves. Inorganic materials have a much smaller temperature and stress-induced area change and the corresponding difference between (4.19) and (4.21) or (4.20) and (4.22) is small.

Another, inconsistency between precise definitions and general practice is sometimes encountered when measurements are reported at voltages considerably greater than zero. Allowing X to represent stress or temperature, the derivative,

$$\frac{\partial D}{\partial X} = \frac{\partial \epsilon'}{\partial X}\ \varepsilon_o E + \epsilon' \varepsilon_o \frac{\partial E}{\partial X} + \frac{\partial P_o}{\partial X} \tag{4.23}$$

has two terms in addition to that in (4.19) and (4.20). The first term involving electrostriction can be large if E is large. From (4.3) and (4.4) this is a legitimate part of p and d which are functions of E. The second term would not appear if E were held constant, but in practice it is the voltage Φ that is held constant and the thickness $s = \Phi/E$ varies with the measurement and gives an electromechanical contribution. Similarly the third term is measured at constant Φ. (Electrostriction and electromechanical contributions are considered in a different way in Ref. [4.36]).

To reduce ambiguity, we will consider measurements made at zero field and for simplicity and a more straight forward comparison of p and d, will use hydrostatic pressure as mechanical stress (positive pressure is a negative stress Without giving the details, [4.35], the straight-forward differentiation of Eq. [4.17] to obtain the pressure and temperature derivatives of surface charge in an

electret gives:

$$A^{-1}(\partial Q/\partial T)_p = -P_o \alpha [\varepsilon_\infty/3 + \phi^2/2 \alpha T + \gamma\phi^2] \quad (4.24)$$

$$A^{-1}(\partial Q/\partial p)_T = P_o \beta [\varepsilon_\infty/3 + \gamma\phi^2] \quad (4.25)$$

where $\alpha = (V)^{-1}\, dV/dT$ is the volume coefficient of thermal expansion, $\beta = -(V)^{-1}\, dV/dp$ is the volume compressibility, $\gamma = -V\omega^{-1}\, d\omega/dV$, is a Grüneisen constant for the dipole torsional frequency ω and ϕ^2 is the mean squared torsional displacement of the dipole fluctuations.

These equations show that for this model most of the piezo- and pyroelectric response comes from volume expansion and its effect on ε_∞. There is an additional contribution from temperature change which can be illustrated with a physical model like that in Fig. 4.8. Although the dipoles have a fixed mean direction, there is always thermal motion whose mean squared amplitude in the simple harmonic approximation is proportional to temperature. Thus increasing the temperature of a dipole reduces the average magnitude of its moment. This effect was the basis of a theory of pyroelectricity in PVDF due to ASLAKSEN [4.37], and accounts for about 1/3 of the pyroelectricity in PVC and possibly a similar fraction in other polymers. The amplitude of molecular librations is difficult to measure or to predict *a priori* because of the large number of vibrational modes and molecular conformations contributing. However, one paper gives a value of 10° for the root mean squared torsional displacement of polyethylene molecules based on x-ray data [4.38].

4.3 Symmetry and Tensor Components

Crystal symmetry is usually considered in discussions of piezoelectricity. An isotropic amorphous material could no be expected to be either piezo- or pyroelectric at zero field because its response to stress will be the same in all directions.

However, of one preferentially aligns molecular dipoles in the specimen, there is no longer a center of symmetry and the sample will be both piezoelectric and pyroelectric. Polymer films, particularly semi-crystalline polymers, are often stretched which preferentially aligns the polymer molecules parallel to the stretch direction and they are then poled to align the dipoles normal to both the stretch direction and the plane of the film. (We consider only those polymers with dipoles normal to the molecular axis). The result is to remove the isotropy present in the plane of the unstretched film. The axes are usually identified as shown in Figure 4.9, which depicts a model of a semi-crystalline polymer. The expected components of the piezoelectric and pyroelectric sensors for such a specimen and their proper signs are:

$$d = \begin{matrix} 0 & 0 & 0 & 0 & d_{15}^{+} & 0 \\ 0 & 0 & 0 & d_{24}^{+} & 0 & 0 \\ d_{31}^{+} & d_{32}^{+} & d_{33}^{-} & 0 & 0 & 0 \end{matrix} \qquad (4.26)$$

$$p = \begin{matrix} 0 \\ 0 \\ p_3^{-} \end{matrix} \qquad (4.27)$$

The assignments can be made by inspection from Fig. 4.9. Stress in the + 3 direction will increase the sample thickness and thus decrease the electrode charge giving a negative d_{33}. The stress in the 1 and 2 directions will decrease the thickness and increase electrode charge, giving a positive d_{31} and d_{32}. Experimentally d_{33} is found to be negative [4.71] and d_{31} and d_{32} predominently positive for PVDF [4.39] and d_{31} is also found to be positive for PVF [4.40]. d was also found to be negative with hydrostatic stress for PVC [4.41]. Remember that we are using the assumption that the electrodes expand with the specimens and that we have adopted equations (4.21) and (4.22) as our definitions. If we use the proper definitions given by equations (4.19) and (4.20) stress in all three directions 1, 2, and 3, is expected to increase the volume and decrease the polarization giving negative d_{3j} components.

Unusual effects may be encountered with highly oriented polymers where the Poissons ratio n_{31} for the ratio of the strain in the 3 direction to the strain in the 1 direction when stress is applied in the 1 direction may be greater than 0.5 and n_{32} may be considerably less than 0.3. These values are the usual limits on n for isotropic materials. This point has been discussed by Sussner [4.42] and may lead to unusual behavior such as a decrease in volume when stress is applied in the draw direction and positive strain in the draw direction with an increase in hydrostatic pressure.

The shear components result because a positive shear about the 1 axis, T_4, rotates the dipoles into the + 2 direction and a shear about the 2 axis, T_5, rotates the dipoles into the + 1 direction. Neither shear causes a change to first order in the moment in the 3 direction. A shear about the 3 axis, T_6, does not change the moment. Because there is no net moment along the 1 and 2 axes, $p_1 = p_2 = 0$ and an increase in temperature produces an increase in volume and decrease in polarization yielding a negative p_3. The $\underline{d}$ matrix constructed from physical arguments for amorphous polymers is characteristic of C_{2v} symmetry. This symmetry is found for the polar crystal phase of PVDF [4.39] and for polar PVF [4.43]. Poled, unoriented polymers should give $d_{31} = d_{32}$ and $d_{24} = + d_{15}$, characteristics of a piezoelectric matrix with $C_{\infty v}$ symmetry [Ref. 4.5, Sect. IA].

4.4 Structure

4.4.1 General

Using the model discussed above, it is possible to hypothesize four requirements for large piezo- and pyroelectricity in polymers. i) There must be molecular dipoles present, the higher their moment and concentration the

better. ii) There must be some way of aligning the dipoles, the more alignment the better. iii) There must be a way of locking-in the dipole alignment once it is achieved, the more stable the better. iv) The material should strain with applied stress, the more strain the better (some of the pyroelectric activity need not result from the strain). Evaluating these conditions for a particular polymer requires considerable data on the molecular and bulk structure and properties. In the following discussion we consider in some detail two different types of synthetic polymers--amorphous and semi-crystalline. Other types--including the important class of bio-polymers which have permanent dipole moments along the molecular axis--will not be considered here. Abbreviations to be used are defined at the beginning of this book.

4.4.2 Amorphous Polymers

Poly(vinyl chloride); (PVC), is an example of an amorphous polymer which can be made piezo- and pyroelectric [4.6, 25, 35, 41, 44]. The repeat unit is polar with an effective dipole moment of 3.6×10^{-30} C.m (1.1 D) [4.45]. The usual form of PVC is amorphous because of the non-stereospecific addition of monomer units during polymerization. More stero-regular (syndiotactic) crystallizable PVC can be made and its crystal structure has been determined [4.46]. PVC is an equilibrium liquid above its glass transition temperature (about 80°C), although thermal decomposition is appreciable above this temperature. Below 80°C, the kinetics of molecular reorganization are slow enough that a non-equilibrium amorphous solid (glass) is formed. Structural relaxation times of the glass increase rapidly with decreasing temperatures to the order of years at room temperature. Thus, this polymer fits all criteria in 4.4.1 for piezo- and pyroelectricity. To illustrate the calculation of p and d we can substitute Eq. (4.15) for P_o in (4.24) and (4.25) because the

dipoles are small enough that the product of their moment times the field is much less than their thermal energy kT and the polarization is linear with field. For more background see [ref. 4.47,p.32].

$$p_y = \Delta\varepsilon'\varepsilon_o E_p \alpha [\varepsilon_\infty/3 + \phi^2/2\alpha T + \gamma\phi^2] \quad (4.28)$$

$$d_p = \Delta\varepsilon'\varepsilon_o E_p \beta [\varepsilon_\infty/3 + \gamma\phi^2] \quad (4.29)$$

We use $\Delta\varepsilon' = 10$ and $\varepsilon_\infty = 3$ [4.45], $\alpha = 2.34 \times 10^{-4}/K$, $\beta = 2.58 \times 10^{-10} m^2/N$ [4.41], T = 300 K and $\phi^2 = 0.07$ rad^2. (from estimate of $\phi = 15°$). The Grüneisen constant is expected to be small because the force constants for dipole rotation are mostly intramolecular and do not depend strongly on volume. Neglecting the small terms in γ, we find $p_y = -0.10$ nC/cm^2 K and d_p -0.73 pC/N when E_p=320kV/cm, in good agreement with measured values [4.48]. The subscript p indicates hydrostatic pressure and the subscript y helps to distinguish the symbol for pyroelectric coefficient from that for pressure.

Even if one does not have dielectric data, one can assume $\varepsilon_\infty = 3$ and the quantity $\Delta\varepsilon$ can then be calculated with reasonable confidence from the dipole moment using Onsager's equation [4.45]. REDDISH [4.45] interpreted the dielectric data on PVC as indicating that the length of the relaxing segments increased as the temperature decreased below T_g and since the $\Delta\varepsilon$ increases linearly with the number of dipoles per rigid unit, large polarizations could be achieved. Unfortunately, we found no enhancement of p and d by lower temperature poling of PVC and suspect the observed effects in dielectric properties are due to space charge.

Since most of the variables in (4.28) and (4.29) will be similar for all polymer glasses, larger coefficients can be sought from polymers with a large dipole moment (p and d will increase as the square of the dipole moment per unit volume) and by increasing the poling field. A possible candidate is polyacrylonitrile (PAN) with a dipole moment greater than 4D. Unfortunately, PAN may have an anomalous liquid phase in which dipole-dipole forces prevent normal polarization [4.49]

contrary to criteria (ii) in Subsect. 4.4.1. In other cases the dipoles may not become immobile at T_g (e.g., polymethylmethacrylate) contrary to criteria (iii) . A thermally stable, high T_g polar glass may have useful high temperature applications, but presently the most sensitive piezo- and pyroelectric polymers are semicrystalline. A comparison of a semicrystalline polymer and PVC is shown in Fig. (4.10).

4.4.3 Seimcrystalline Polymers

The most interesting of the semicrystalline polymers are PVDF, PVF and related copolymers. These polymers crystallize because the fluorines, unlike larger chlorines, are close enough in size to hydrogen so as not to interfere with regular packing. Both polymers have head-head and tail-tail defects, where successive repeat units are backwards. Typically, these amount to 5% for PVDF [4.50-52] and 25-32% for PVF [4.50]. A h-h unit in PVDF is immediately followed by a t-t unit [4.50] so that 5% of these defects cancel 10% of the dipole moment of the planar zig-zag chain.

The dipole moment of PVF could be quite large in the trans planar conformation if all fluorines were on the same side of the C-C plane (isotactic). For atactic PVF the average moment will be in the C-C plane, perpendicular to the molecular axis and close to 1/2 that of PVDF. However, 30% h-h defects will reduce the net moment of the planar PVF by about 60%, with the result that the net moment of trans PVF is about 20% that of trans PVDF.

Semicrystalline polymers consist of lamellar crystals mixed with amorphous regions. A schematic diagram of a spherulite within an unoriented semicrystalline polymer is shown in Fig. 4.11. Annealing or crystallizing for longer times, at higher temperatures and pressures increases the lamellar thickness and

perfection which results in a higher sample density. The crystals grow in the form of spherulites and studies of the morphology of PVDF show that three crystal phases have distinct morphology and can grow simultaneously from the melt or one phase can grow at the expense of another [4.53-55]. A typical molecular weight for these polymers is 10^5 for an extended length of 0.5μm and a total of 2000 repeat units.. Since the lamellae are of the order of 10^{-8}m thick, a single molecule folds back and forth through the same or different lamellae many times. When stretched to several times the original length, the specimen becomes oriented such that the lamellae are normal to the stretch direction and the molecules are parallel to the stretch direction [4.56,57]. The polymers currently of greatest interest for piezoelectric applications, PVF and PVDF are of the order of 50 to 70% crystalline. [4.51,58,59]

The amorphous phase is probably mostly confined to layers between the crystal lamellae. The nature of this phase and the degree to which it is oriented and connected to the crystals is a subject of debate. The amorphous phase seems to have normal supercooled liquid properties with a liquid-glass transition region around -50°C, and a Williams-Landed-Fetty type dielectric relaxational behavior [4.18,60,61]. Broad line NMR [4.60-63], and mechanical relaxation data [4.5, 39, 51, 62, 64] also show a normal liquid-glass relaxation. The magnitude of the associated dielectric dispersion and room temperature relative permittivity increase with amorphous content as expected [4.61,62].

The dielectric permittivity is quite sensitive to uniaxial and biaxial orientation of the film [4.65], the more orientation the higher the polarizability normal to the draw-direction. This effect is typically used to enhance the

permittivity of PVDF film used in capacitors and has been attributed to orientation of the liquid material so that rotations about the amorphous molecular axes are more effective in contributing to the polarization. An alternative explanation by Davies et al [4.66] is that since orientation aligns crystal lamellae normal to the draw direction, the liquid-crystal layers are parallel to the applied field giving a mean permittivity larger than in an undrawn specimen where some lamellae are normal to the applied field and their permittivities add in series. From criteria (iii) in Subsect. 4.4.1 we do not expect the amorphous phase to contribute to piezo- and pyroelectricity in PVDF and PVF. MURAYAMA [4.9] has stated the same conclusion.

Three crystal phases have been reported for PVDF. The α phase (alternatively form II) forms most readily upon cooling the molten polymer and assumes a conformation close to trans-gauche-trans-gauche' which then packs in the unit cell to yield an antipolar crystal [4.67,68]. Mechanical orientation of the α phase at temperatures below 50°C yields the β phase (form I) which has an extended all-trans (planar zig zag) conformation and packs in the unit cell with the dipole moments of adjacent chains parallel to yield a polar crystal [4.57,67]. A third form, referred to as γ or form III can be obtained by crystallization from selected solvents such as dimethylsulfoxide or dimethylacetamide [4.69] or by annealing at high temperatures [4.53,54,70]. The infrared spectra of form III closely resembles that of form I so an all-trans conformation was assumed [4.71] to aid in the indexing of x-ray diffraction spacings [4.72]. More recent data may require modifying the present conclusions regarding form III to account for a spacing along the chain which is double that exhibited by the α phase [4.73]. For example, a gtttg'ttt conformation would account for the c-axis repeat and the trans sequences would make it vibrationally similar to that of β phase. Projections of the α and β conformations onto a plane normal to the

molecular axes are shown in Fig. 4.12. The crystal structure of PVF is the same as the β phase of PVDF [4.43] and mixtures and copolymers of these two monomers tend to cause crystallization into the polar β phase [4.74]. Model p calculations have been made for comonomer units and head to head defects within PVDF and their effects on the potential energy of chain conformations [4.75] are consistent with experimental observations.

The repeat unit for PVDF, $(-CF_2-CH_2-)_x$, is assumed to have a dipole moment close to that of difluoroethane [4.76] which is 7.56×10^{-28} Ccm (2.27D). In the all-trans conformation (planar zig-zag) the component of this moment normal to the long molecular axis is about 6.9×10^{-28} Ccm (2.1D). In the α phase $tg\bar{t}g'$ conformation the same 2.27D per repeat unit, using the atomic coordinates of reference [4.72] yields a dipole moment of $\mu_\perp^\alpha = 4.03 \times 10^{-28}$ Ccm perpendicular to the long axis and $\mu_\parallel^\alpha = 3.36 \times 10^{-28}$ Ccm parallel to the long axis. The antipolar unit cell does not have proper symmetry to yield piezo- and pyroelectric activity. However, recent x-ray data shows that the antipolar unit cell can be transformed by a large electric field to give a stable polar modification of the $tg\bar{t}g'$ conformation which is then both piezo- and pyroelectrically active [4.77]. This finding modifies earlier conclusions that the β form is necessary for activity.

The usual methods of identifying the fraction of crystallinity in a specimen are to compare its density to that of crystal and amorphous densities [4.78] or to compare its heat of fusion to the crystalline heat of fusion [4.78]. The usual measures of crystal phase fractions are x-ray diffraction [4.79] and infra-red absorption [4.70] intensity ratios.

4.5 Properties of Semicrystalline Polymers

4.5.1 Crystal Relaxations

In the crystal phases of PVF and PVDF the question of rotational freedom of the dipoles is crucial [Subsect. 4.4.1, ii]. Ample dielectric relaxation data exist on PVF [4.80] and α phase PVDF [4.18, 61, 78, 80-83] and mechanical data on PVF [4.64] and α phase PVDF [4.62] and thermally stimulated current (TSC) data on α phase PVDF [4.18] to conclude that a crystal relaxation α_c occurs at about 80°C at a measuring frequency of 100 Hz. At room temperature the relaxation time τ_c for the α_c relaxation is increased to about 1 sec. Log τ_c is linear with 1/T and the activation energy is around 100 kJ/mol. The β phase of PVDF is reported to have a mechanical crystal relaxation at 110°C at 10 Hz [4.39, 62]. Its activation energy has not been determined. Dielectric α_c relaxations in β and γ phase PVDF are generally not observed possibly because of rapidly increasing ε' and ε'' with temperature. This behavior is usually attributed to space charge effects [4.80, 82, 83]. TSC data give strong background currents even from unpoled specimens [4.12, 84]. At lower temperatures current with a broad maximum at 80°, and integrated charge of up to 3 $\mu C/cm^2$ is observed [4.21]. Davies has reported [4.85] that after removing a large fraction of mobile charges by application of a large DC field (field cleaning) the α_c relaxation in β phase PVDF was observed at about 140°C and 10Hz. The activation energy was about 100 kJ/mol. That the dielectric α_c is a crystal relaxation was shown for α phase PVDF by the dependence of its amplitude on crystallinity and by observing its disappearance at the melting temperature [4.61]. That it can exist in the β phase is demonstrated by its presence in PVF [4.80], observed following field cleaning. The relaxation probably involves rotation of an entire intralamellar segment with twisting at the lamellae surfaces analogous to the well documented α_c mechanism in PE [4.86]. Since twisting must be about

C-C bonds, these rotations would be restricted by the crystal fields of neighboring molecules. This rigid-rod model is also supported by the dependence of the α_c relaxation parameters on molecular thickness [4.60, 78, 82]. However, some evidence has been reported that the polarization of the α_c relaxation in α phase PVDF is along the C crystal axis contrary to the usual case [4.87]. Additional direct evidence for electric field induced rotation of molecules in the crystal phase of PVDF is discussed in Subsect. 4.5.2.

It is useful to review linear relaxation theory before proceeding to non linear effects at high field. The crystal relaxation occurs by rotation of the molecules about their long axes within lamellar crystals either by rigid rod rotation or twisting [4.86]. To simplify the calculation we assume the crystal lamellae are thin slabs aligned normal to the polymer film as expected in most commonly measured films from uniaxial or biaxial orientation. The net sample polarization P_s arises from the average of the crystal P_c and the liquid P_ℓ polarizations

$$P_s = \Psi P_c + (1-\Psi)P_\ell \tag{4.30}$$

where Ψ is the crystal volume fraction.

Since $P = (\epsilon'-1)\epsilon_o E$ and the field, E, for these oriented thin lamellae will be the same inside and outside the crystal (tangential component of E continuous across the crystal-liquid interface) we can write the sample permittivity as a simple sum of the crystal ϵ_c and liquid ϵ_ℓ permittivities

$$\epsilon_s = \Psi\epsilon_c + (1-\Psi)\epsilon_\ell \tag{4.31}$$

At radio frequencies well above the glass transition temperature the relaxation amplitude of the sample is

$$\Delta\varepsilon_s = \Psi\Delta\varepsilon_c \tag{4.32}$$

where $\Delta\varepsilon$ is the difference between relaxed and unrelaxed values of ε. To relate $\Delta\varepsilon_c$ to microscopic quantities we adopt the familiar 2-site model [4.86] with an important modification to allow for the cooperative effects common to ferroelectric materials.

Assume a molecule in the crystal has its most probable orientation with its dipole moment m_o at an angle θ with respect to an applied electric field E. A second possible orientation (site 2) is at an angle $\theta + \pi$ and the lattice potential energy of a molecule in site 2 is greater than in site 1 by the energy U as indicated in Fig. 4.13 in which θ=0. The probability of occupation of site 2 will be $f_2 = C\exp[-(2U + 2m_oE\cos\theta)/kT]$ and that of site 1 will be f_1=C where C=1/1+exp[-(2U+2m_oEcos θ/kT]is a normalization factor chosen so that $f_1 + f_2 = 1$, and $2U + 2m_oE\cos\theta$ is the work to move one segment from site 1 to site 2 [4.88]. (The term 2U includes the work to move a molecule from site 1 to site 2, plus the work to adjust the energies of the remaining molecules.)

Let m be the apparent dipole moment per molecule for any arbitrary distribution of dipoles between sites 1 and 2 in a given crystallite. For such a crystal, the average moment in the direction of the field will be:

$$m\cos\theta = m_o\,[\,f_1\cos\theta + f_2\,(\cos\theta + \pi)] = m_o\,(f_1 - f_2)\cos\theta \tag{4.33}$$

whence,

$$2m_o\,E(\cos\theta)/kT = -2U/kT + \ln\,[(1+m/mo)/(1-m/m_o)] \tag{4.34}$$

The cooperative aspects of this model arise from the requirement that the system normally ordered in site 1 is equivalent to the same system normally ordered in site 2, and that if both sites are equally populated then sites 1 and 2 must have equivalent energy. That is, the energy U must depend on the values of f_1 and f_2. The type of dependence which has been applied to theories of ferromagnetism [4.89], Bragg-Williams order-disorder transitions in alloys [4.90] and ferroelectricity in Rochelle salt [4.91] is:

$$U = U_o (f_1 - f_2) = U_o (m/m_o) \tag{4.35}$$

where U_o is the lattice energy difference between site 2 and 1 when site 1 is completely populated ($f_1=1$, $f_2=0$).

Using this result in (4.34) we have an important relationship between the average moment of a dipole in this crystal and the applied field, or

$$2m_o^2 E \cos\theta / kT = -2U_o m/kT + m_o \ln [(1+m/m_o)/(1-m/m_o)] \tag{4.36}$$

To find $\Delta\varepsilon_s$ we need to calculate the change in sample moment with electric field. The differential of (4.36) at E=0 gives:

$$(\partial m/\partial E)_{E=0} = 4f_1 f_2 [1-2f_1 f_2 \ln (f_1/f_2)/(f_1-f_2)]^{-1} m_o^2 \cos\theta/kT \tag{4.37}$$

This result differs from that usually obtained for the 2 site model [4.92] by the additional term in brackets (due to the cooperativity), and the absence of the term $3\varepsilon_\ell/(2\varepsilon_\ell + \varepsilon_c)$ due to the assumption of lamellae rather than spheres. It leads in a straightforward way [4.47] to the result:

$$\Delta\varepsilon = \psi(N/V)4f_1f_2[1-2f_1f_2\ln(f_1/f_2)/(f_1-f_2)]^{-1}\ \mu_o^2(\varepsilon_c+2)^2/18kT \qquad (4.38)$$

where $\mu_o=3m_o(\varepsilon_c+2)^{-1}$ [4.92] is the vacuum moment of the molecular segment involved in the rotation, ε_c the non relaxed relative permittivity of the crystal, N/V is the number of crystal dipoles per unit volume, ψ is the volume fraction crystallinity, and the average of $\cos^2\theta$ for single axis rotators with the axes in the plane of the film is ½. The main features of the result are that, for a given f_1, the relaxation amplitude is larger than for the non-cooperative (constant U) case tending towards infinity at $U_o/kT=1$.

Very high dielectric constants are sometimes reported for PVF and PVDF [4.80, 93] but these are usually attributable to space charge effects which can be greatly reduced by application of high DC fields to the sample [4.80]. It is probable that the enhancement of ε_s near the Curie temperature due to dipole disordering has not yet been observed because the Curie temperatures expected for PVF and PVDF are well above the temperature at which these crystals melt. Equation (4.38) should be replaced by a more general equation for conducting dispersions and random orientation of lamellae when necessary. Note that the amplitude of the crystal and liquid relaxations as measured will appear smaller than if measured in each phase separately because of the facter ψ.

Since the pertinent data are available for PVF, it is instructive to apply the above model to this polymer. A typical all-trans segment within the lamellar crystal can be expected to contain about 40 repeat units. 60 percent of these are nonpolar because of head to head defects and their effective rigid-rod moment (μ_o) will be $16 \times 3.3 \times 10^{-28}$ C cm. The number of such rods per unit volume is $1.8 \times 10^{22}/40$ cm^{-3}, and T = 350K.

The typical commercial films of PVF are highly oriented and have a crystallinity around 50 percent [4.59]. We can use Eq. (4.38) and data from ref.[4.80] which shows $\Delta\varepsilon_s \approx 5$ to calculate f_1 and from the definition of f_1 at E=0 obtain the difference in crystal energy for disordered and ordered molecules. Eq. (4.36) yields a fraction of disordered molecules of 5 percent (an alternative solution, f_1 = 50%, is not stable [4.88]) when $U_0/kT=1.67$. That is, even though PVF has a polar, transplanar crystal structure at a temperature of 350K approximately 5% of the molecular segments in the crystal lamellae will be oriented with their net moments opposite that of the host lamellae. This is a dynamic disorder such that all segments spend about 5% of the time in the antipolar orientation. The angular frequency with which a segment changes orientation and the potential energy barrier which must be traversed, W, are calculable from the simple Arrhenius expression:

$$\nu = 2\nu_0 \exp(-W/kT) \qquad (4.39)$$

where ν_0 is the librational frequency of the segment in the crystal (about 2×10^{12} Hz for β phase PVDF [4.94]). From dielectric data at 100 Hz and 350K, W/kT = 24 for PVF [4.80]. Both U_0 and W will depend on pressure and temperature decreasing by about 10 percent for each 1 percent increase in crystal volume [4.95]. Even at room temperature the relaxation time for dynamic disordering of the crystal is of the order of seconds with several percent of the crystalline segments antipolar to the crystal moment at any instant.

Qualitatively similar behavior is expected to occur in β phase PVDF except that nearest neighbors are antipolar in the ordered state and the disordered state consists of several percent polar nearest neighbor pairs. The absence of published dielectric data on the α_c relaxation in β phase PVDF makes quantitative analysis of this case unclear, but there is little doubt that the same type of dynamic crystal disordering typical of semicrystalline polymers is present.

It is important to distinguish between the linear response of the dynamic disordering of molecular segments in the PVDF crystal to changes in applied electric fields at the low voltages usually employed for dielectric measurements and the non-linear response expected at the high voltages used to polarize piezo- and pyroelectric samples. The linear low-field response does not involve permanent changes in polarization while the high field response leads to ferroelectric reorientation.

4.5.2 Ferroelectricity

PVDF in the polar form is often supposed to be a ferroelectric [4.96, 97], which means that it is not only a polar crystal but that the stable equilibrium crystal polarization can be reoriented with an applied electric field. Direct evidence for a field induced change in the unit cell orientation in PVDF measured by x-ray pole figures has been reported [4.22, 98]. Molecular orientation measurements using Raman techniques suffer from the dilution effect of the liquid phase [4.99]. The usual hysteresis measurements [4.12, 100] of charge vs. field are difficult because of space charge effects and the results are ambiguous. Measurement of piezoelectric [4.12, 36] and pyroelectric [4.93] response as the field is cycled from large positive to negative values does give a hysteresis loop. A poled PVDF film was shown to require 450 kV cm^{-1} to suppress its piezoelectric response [4.36]. High dielectric constants of the order of 1000 [4.93] are also indicative of ferroelectric switching in PVDF and PVDF-TFE copolymer but since this behavior can often be eliminated by annealing in the presence of a DC field [4.80,101], space charge effects rather than ferroelectric switching is probably responsible.

In the work of Kepler and Anderson [4.98] referred to above, they assumed the

molecular segments could rotate about their long axes and occupy any of six orientational positions at $\pi/3$ radians apart. They found that the length of a rotating unit was 40 CF_2-CH_2 repeat units which is about the same as the number of units in one molecular segment in the crystal. They also reported that the crystal alignment was partially lost by high temperature annealing. Fukada et al [4.102] used polarized infrared absorptions for symmetric and antisymmetric CF_2 stretch vibrations to show that these dipoles orient in an electric field. Their results indicated that the relationship between piezoelectricity and dipole orientation was not unique. Since they measured the average $\langle\cos^2\theta\rangle$ rather than $\langle\cos\theta\rangle$ (where θ is the angle between the dipole moment and electric field) it is possible that non-uniform polarization which is commonly observed at lower poling voltages[4.19.30]is an important factor. Infrared measurements of crystal dipole orientation at lower frequencies were also reported to show hysteresis [4.103]. That is, CF_2 dipoles in the crystal do align with an applied field and some of the alignment persists until a strong field is applied in another direction.

Not only does field induced alignment of dipoles occur but conversions from one non-polar phase to at least two other polar crystal phases has been demonstrated [4.77, 104-108]. These and other results [4.12, 100, 109] provide strong evidence for ferroelectric switching in the crystal phase of PVDF. It is still possible, however, that not all of the piezoelectric and pyroelectric activity in PVDF is due to oriented dipoles and the possibility that trapped space charges are an important factor is often suggested [4.10, 16, 110].

According to Eq. (4.36) we can calculate the dipole moment for a cooperative 2 site model of PVDF as a function of electric field. The results are shown in Fig. (4.14) for several values of the parameter U_o/kT. We can write the free energy difference between the partially ordered system and the completely disordered system as,

$$A(m/m_o)-A(o) = -U_o(m/m_o)^2/2-mE\cos\theta+(kT/2)[(1+m/m_o)\ln(1+m/m_o)+(1-m/m_o)\ln(1-m/m_o)] \quad (4.40)$$

The extrema of A-A(o) are given by letting $\partial[A-A(o)]/\partial(m/m_o) = 0$ which gives Eq.(4.36). The values of [A-A(o)]/NkT for E=0 are given in Fig. (4.15) as a function of m/m_o for several values of U_o/kT.

The ferroelectricity of the model arises for $U_o/kT > 1$ because of the existence of two minima in the free energy corresponding to positive and negative values for the crystal moment. The system can be switched from +m to -m by application of a sufficiently high electric field in a direction opposite m as illustrated in Fig. (4.16) for the case $U_o/kT = 1.5$. At a value of $m_oE/kT\approx0.2$, the minimum at $m = -0.95m_o$ is removed and the only remaining minimum is at $m > +0.95m_o$.

Physically then we can describe poling of PVDF in terms of Fig. (4.14) as follows. When a large field is applied to the specimen such that E is considerably greater than its critical value E_c given by the point of infinite slope in Fig. (4.14), the moment of the crystal will be positive. If the field is then decreased beyond $-E_c$, the stable solution for positive m disappears and m switches to a negative value. This procedure of cycling E from large positive to negative values results in a hysteresis curve ideally given, for example, by the dashed path shown on the $U_o/kT = 1.5$ curve of Fig. (4.14).

In the case of PVF we saw that dielectric data yields $U_o/kT=1.7$ so that $m_o E_c/kT=0.3$ and, using the moment given in Subsec (4.5.1), $E_c=0.3$ Mv/cm. This number is quantitatively similar to the lowest fields used for poling PVF and PVDF, and gives some indication that a simple cooperative model is realistic.

4.5.4 Space Charges

Space charge measurements are frequently made by measuring the currents generated by heating, at a uniform rate, a specimen with evaporated electrodes which has previously been cooled under an applied field. The thermally-stimulated short-circuit currents (TSC) result from dipole reorientation and from the change in the dipole moment of the space charge distribution [4.111]. Studies on both amorphous and semicrystalline polymers have shown the space charge to be predominantly positive near the negative poling electrode and negative near the positive poling electrode (heterocharged electret). Kerr effect measurements in liquid nitrobenzene with dc fields show uniform space charge distributions with a net positive charge density of the order of 10^{-8}C/cm^3 [4.112]. (For a further discussion of such observations, see Subsect. 1.7.3). Dielectric measurements of PVF and PVDF typically show anomalously high values of ε' at high temperatures and low frequencies [4.80, 83, 113]. This effect is generally attributed to ionic space charges [4.83]. It was shown that the interfacial polarization in solid PVDF is different from the electrode interfacial polarization effects in liquid PVDF and was attributed to space charge polarization at the liquid-crystal interfaces [4.83]. In TSC measurements it was shown that repeated cycling of PVDF from 25 to 100^{o}C with an applied field, reduced the space charge effects [4.18]. Space charge concentrations in liquid nitrobenzene [4.112], and the space charge effects seen in dielectric measurements of PVDF [4.80, 83, 113] and PVF [4.80] were also reduced by application of dc fields for several hours. This reduction partially recovers with time after removal of the field. At

very high fields (E>500kV/cm) there is a change in the above behavior and current tends to increase with time at constant voltage leading ultimately to breakdown [4.114].

The general behavior of a conducting liquid with dispersed crystals of roughly equal volume is quite complicated [4.115]. EMF's generated by chemical or electronic interactions between a polymer film and the metal electrodes [4.116] are a possible source of anomalous effects such as the extremely high isothermal short-circuit currents observed in vinylidene fluoride polymers at high temperatures [4.117] and variations in current-voltage behavior with electrode metal [4.80, 118]. If, as seems certain, ferroelectric switching of the polar crystals occurs during the early stages of poling, then continued poling results in a flow of charge, mostly through the more conductive liquid phase regions with positive charges moving toward the negative electrode and negative charges toward the positive electrode. At normal poling temperatures ($\sim 100^{o}C$) the current is time dependent and bulk interfacial polarization effects are evident [4.83]. The charge carriers could tend to pile up at the crystal surfaces where their normal drift is hindered as shown in Fig. 4.17. Electric fields from oriented crystal dipoles would tend to trap these charges at suitable crystal-liquid interfaces. This situation is analogous to concentrated emulsions of oil and water [4.119]. TSC results show that space charges are released at temperatures higher than the dipole relaxation maxima and these for PVDF are considerably above room temperature [4.111, 120]. As a result, when the specimen is cooled to room temperature the charges are immobilized and remain at the crystal surfaces as in Fig. 4.17. The space charges form a dipole which has the stiffness of the crystal and because of non-uniform strains will produce a piezo- and pyro-electric response [see Subsect. 4.2.2]. Note however, that the space charge dipoles if formed from interfacial polarization of the poling-current charges are opposing the molecular dipoles and will reduce the piezo- and pyroelectric response.

The observation of a slow poling process reported for PVDF [4.10, 36, 103], whereby the piezoelectricity slowly increases with time, and the observation that space charges are removed by dc fields on a similar time scale [4.18, 80, 83, 112, 113] support the idea that a decrease in space charge reduces the masking effects of space-charge dipoles. Also the partial decay of piezoelectricity with time after removal of the field [4.10] and the partial recovery of space charge density with time [4.80, 83, 113] may be similarly related to the postulated space-charge dipoles.

Probably the most important role of space charge is in the poling process. It is well known that space charge in a material has associated with it an electric field which will cause the local electric field in the material to be greater or less than the applied field [4.121, 122]. If for example a negative space charge is present in the polymer, the potential difference between the negative electrode and the interior of the polymer will be less than that for an uncharged polymer and correspondingly greater at the positive electrode. Thus, if the polarization due to crystal alignment increases with the local poling field, then the polarization will be greater at the positive electrode for a negatively charged polymer. The distribution of activity in PVDF has been measured and found to be greater at the positive electrode [4.19, 110]. Higher temperatures, longer poling times and higher electric fields reduce this non-uniformity [4.19]. It is surprising that the polarization in PVF tends to be greater at the negative poling electrode [4.123]. Assuming that non-uniform polarization in these materials results from space charge in the bulk polymer, then we conclude that PVDF accumulates a net negative space charge and PVF accumulates a net positive space charge. This charging phenomena is sometimes discussed in terms of a work function difference between the polymer and metal electrodes [4.124-126], which in turn depends on the detailed molecular structure [4.124].

The distortions in local poling fields due to space charge tend to become small at high fields (>1MV/cm), and while studies of space charge effects are necessary for a complete understanding of PVDF, it seems likely that the presence of space charge is not a major factor in the behavior of well poled PVDF.

4.6 Measurements and Data

Piezo-and pyroelectric measurements on polymer films are usually made by applying tension to a strip of polymer and measuring on opposing electrodes the short-circuit charge or open circuit voltage due to a change in the tension. The stress and strain are measured with a load cell and strain gauge and the stress is usually sinusoidal. This basic technique has been discussed previously [4.5, 7]. Measurements can be made by clamping a sample in a vise in series with a load cell. Noise can be reduced for these measurements by the use of good contact electrodes (e.g., evaporated). A double film sandwich with the high potential electrodes together and shielded by the outer grounded electrodes greatly reduces noise problems. Piezoelectric measurements have also been made by applying a field to the specimen and observing the length and thickness change [4.17], by analyzing the response of a piezoelectric film driven electrically in the neighborhood of its resonant frequencies [4.13] and by applying hydrostatic pressure to the film with He gas [4.41]. Pyroelectric measurements are conveniently made by changing the temperature of the specimen and measuring the charge produced [4.41] correcting for any irreversible effects. Heating and cooling can be done with a Peltier device [4.127] which is noisier than a heater or, for electromagnetic purposes, with optical radiation [4.20]. A very convenient dielectric heating method has recently been demonstrated [4.128]. The accuracy of piezoelectric data is hard to assess since error analyses are seldom mentioned. Piezoelectric and electrostriction data on PVDF as a function of temperature and frequency have been adequately reviewed previously [4.5,7,10].

There are many reports in the literature of piezoelectric and pyroelectric response from PVDF as a function of poling conditions. A summary of all of them would be complicated because there are so many parameters, each of which can be varied over a wide range, and conclusions drawn from one set of measurements are not valid for other values of the parameters. For example, early data [4.10] on samples with different contents of form I and form II crystals when poled at 320 kV/cm and 40°C showed a variation in piezoelectric response of more than 100 fold, implying a need for the presence of polar form I in order to obtain good piezoelectric response. Subsequent poling [4.13] of oriented form II at slightly higher fields yielded films with piezoelectric coefficients as much as one-half as large as those from form I. More recently [4.105] it has been shown that electric fields in the vicinity of 1 MV/cm can cause a crystal phase change from antipolar form II to a piezoelectric polar form II and at higher fields, an additional phase change to form I occurs. Again, early data [4.10] showed a strong dependence of electrical response on poling temperature for poling times of 30 minutes at 1 MV/cm. More recent data for much longer times (10^3 min.) implies that the ultimate response from a given sample depends only upon applied field and that temperature merely affects the rate at which polarization occurs [4.129]. In measurements of pyroelectric response the uniformity of polarization increased significantly when the poling time was increased from 5 to 30 minutes [4.19].

Polarization vs. time measurements for PVDF show two stages according to several authors [4.10,103,110,130]. Some [4.10,103,110] report a fast response at less than a second and a slow response at 1-2 hours, while others [4.130] report the fast response at 1 minute and the slow response at 1 hour.

More recently it has been shown that for stronger electric fields (in the vicinity of 2 MV/cm), the polarization occurs within the first few seconds of poling--even at room temperature [4.105, 108, 114]. The nature of the electrodes or the presence of charge carriers can influence the uniformity of polarization over certain ranges of the variables mentioned above. In general, high fields and longer poling times lead to uniform polarization [4.19].

There is disagreement about whether polarization saturates at high temperatures and high fields. Murayama et. al. [4.9, 10] reported no saturation for the piezoelectric response in PVDF and Day et. al. [4.19] report none for the pyroelectric response (although the data for only uniformly poled samples do show saturation effects) [4.19]. Other data show saturation of the piezoelectric response [4.39] in PVDF and in our laboratory both the piezoelectric and pyroelectric response of PVDF and VDF-TFE copolymers saturated as functions of field and temperature [4.48, 114]. Of course, the response also depends upon the orientation of the polymer chains in the film before poling and the direction in which the film is strained while measuring the electrical response. Despite the apparent inconsistences in the details of the poling process, many reports agree that the maximum value of d_{31} for PVDF which has been obtained so far is 15 to 20 pC/N [4.13, 56, 109, 114, 131] and the corresponding pyroelectric coefficient is 3 to 4 nC.cm^{2}K. [4.19, 108, 114, 132, 133] These values are compared with the electrical response from other piezoelectric and pyroelectric materials in Table I. At present there have been few reports of detailed measurements on a single specimen to yield several components of the piezoelectric tensor (Sec. 4.3).

Applications of polymer transducers for reflectivity measurements [4.139], a photocopy process [4.151], radiation detectors [4.20], night vision targets [4.132], intrusion and fire detectors [4.140], hydrophones [4.141], earphones and speakers [4.11], pressure sensors, strain gauges and many more are being

developed or investigated, and the list of applications is growing rapidly, as discussed in Chapter ( ). Several recent relatively non-technical publications have stimulated widespread interest in piezoelectric polymer devices [4.142-144]

4.7 Dipole Model Applied to Semicrystalline Polymers

Evidence for the presence of preferentially aligned crystal domains giving PVDF a net dipole moment has been given in Subsec. 4.5.2. It is important to know if aligned crystal domains can account for the observed activity. A model similar to that for amorphous polymers (Subsec. 4.2.3) has been analyzed [4.145]. In the model the polymer is assumed to consist of crystal lamellae dispersed in an amorphous liquid and oriented approximately normal to the large film surfaces. The molecular segments are preferentially aligned so that their dipole moments are parallel. A typical crystal is assumed to be as shown in Fig.(4.18), with the crystal moment at an angle θ_o with respect to the film surface and an equilibrium amount of real charge trapped at the crystal surfaces which are normal to the crystal moment. Calculation of the charge dQ appearing at the film surface as a result of changes in temperature dT or hydrostatic stress - dp, leads to the following equations for piezo-and pyroelectric response:

$$d_p = \frac{1}{A}\frac{dQ}{dp} = P_o\,\beta_c[(\varepsilon_c - 1)/3 + \phi_o^2\,\gamma/2 + \partial(\ln \ell_c)/\partial(\ln v_c)] \qquad (4.41)$$

$$p_y = \frac{1}{A}\frac{dQ}{dT} = -P_o\,\alpha_c[(\varepsilon_c - 1)/3 + \phi_o^2(\gamma + (2T\alpha_c)^{-1})/2 + \partial(\ln \ell_c)/\partial(\ln v_c)] \qquad (4.42)$$

Where the polarization from crystal dipoles is

$$P_o = \phi(\varepsilon_c + 2)\,N\,\mu_o\,J_o\,(\phi_o)\,\langle\cos\theta_o\rangle/3V_c \qquad (4.43)$$

For the case of no counter charge the crystal length ℓ_c is replaced by the sample thickness ℓ_s. The equations were evaluated using the following experimental values: Temperature, T = 300K, volume expansion coefficients for the crystal $\alpha_c = 1.7 \times 10^{-4} K^{-1}$ [4.146] and sample $\alpha_s = 4.2 \times 10^{-4} K^{-1}$ [4.146]; volume compressibilities for the crystal $\beta_c = 1.1 \times 10^{-10} Nm^{-2}$ [4.147], and sample $\beta_s = 2.39 \times 10^{-10} Nm^{-2}$ [4.148] crystal relative permittivity, $\varepsilon'_c = 3$ [4.35, 62], volume fraction of crystals, $\psi = 0.5$ [4.149], crystal (vacuum) polarization for Form I, $Nu_o/V_c = 12 \times 10^{-6}$ Ccm^{-2}, $d_p/P_o = 2 \times 10^{-6} cm^2 N^{-1}$ and $p_y/P_o = 4 \times 10^{-4} K^{-1}$ [4.105]

The agreement between this calculation and experiment is excellent if one assumes negligible amounts of space charge at crystal-amorphous interfaces. Even with an equilibrium amount of space charge (which gives a contribution opposite that of the dipolar crystals), the model still accounts for about 75 percent of the observed activity in PVDF. Apparently, the largest contribution comes from changes in film thickness with changes in temperature or applied stress. This mechanism is very similar to that for amorphous polymers considered in Subsec. 4.2.3. Also, the predicted ratio of piezo- to pyroelectric coefficient of $d_p/p_y = 50$ K $cm^2 N^{-1}$ is in excellent agreement with experiment and strongly supports the concept that both effects arise from the same basic mechanism, i.e. thermally or mechanically induced dimensional changes in the PVDF film. This type of piezoelectricity is usually called secondary piezoelectricity [4.134]. Kepler has analyzed how much of the pyroelectricity in PVDF is associated with the secondary piezoelectricity and has concluded that no more than half of the pyroelectricity in PVDF arises from the mechanism of secondary piezoelectricity [4.150], in contrast to our conclusion above. His results depend on an assumption of isotropic mechanical properties for biaxially or uniaxially drawn films of PVDF. However, Poisson's ratio of semi-crystalline polymers, for example, is known to vary greatly with orientation [4.42].

The calculated maximum polarization obtainable with a β phase PVDF crystal is about $22\mu C/cm^2$ (the often quoted value of $13\mu C/cm^2$ is calculated from vacuum moments and does not include the effect of the crystal environment). The corresponding maximum values of d_p (max) and p_y (max) are 44 pC/N and 9 nC/cm^2K, respectively. These are more than double the typical values measured for well poled samples where d_p (typical) = 15 pC/N and p_y (typical) = 3.5 nC/cm^2K. This difference between predicted ideal single crystal values and observed values is similar to the difference between piezoelectric coefficients and polarization of $BaTiO_3$ single crystals and powders [4.151], and can be attributed to inefficiency of the poling process in a polycrystalline sample.

The model described above applies to any polar phase of PVDF including polar α phase, and β and γ phases. Probably, there will not be a significant difference in activity for various phases, because of compensating effects. For example, increased compressibility of the polar α phase relative to β phase [4.152] crystals will increase p_y and d_p in partial compensation for the decrease in p_y and d_p due to the decreased moment of the α phase repeat unit.

In many applications the electrical response across the film thickness to a change in the uniaxial stress (d_{31} or d_{32}) is of primary concern. Eq. (4.41) can be modified by replacing hydrostatic stress (-p) with the appropriate stress, T_1 or T_2. Because of the sensitivity of Poisson's ratio to orientation, the change in film thickness will be much greater for a stress in the draw direction T_1 than for a stress transverse to the draw direction, T_2.

Poisson's ratio is also a strong function of amorphous state of the polymer, being closer to normal values $1/3 < \eta < 1/2$ below T_g (about -40^oC) and being outside this range above T_g. In spite of the apparent importance of η to the basic mechanism of piezo- and pyroelectricity in PVDF (that is, the change in sample thickness) [4.145], there are yet no reported data for η. This is due in part to

the difficulty in measuring strains in the thickness of thin films. However, we can estimate from measured values of Youngs modulus $Y_1 \approx Y_2 \approx 2.5 \times 10^9$ N/m^2 [4.39, 131] and assumed values of $n_{31} = 0.6$ and $n_{32} = 0.1$ that $d_{31} \approx 2d_p$ and $d_{32} \approx 0.4\ d_p$. This large difference between d_{31} and d_{32} has been shown experimentally [4.7,13,39] and has been interpreted as evidence for a model where stress along the molecular axis causes dipole alignment and hence an increase in polarization. Here we suggest that differences in the thickness change is the dominant effect.

Other models for piezoelectricity in PVDF include gradual stress-induced melting and crystallization of preferentially aligned crystals [4.153], orientation of dipoles in an anomalous liquid phase [4.154], and increased perfection of the planar zig-zag structures [4.13] both by applied stress. Calculations on the polarization kinetics using several models for PVDF have been made [4.155].

4.8 Summary and Conclusions

Some polymers can be made both piezo- and pyroelectric by suitable application of a large electric field. This effect is true piezo- and pyroelectricity rather than electrostriction, conduction, electromechanical effects, or the motion of conductors in the field of space charges. Two distinct types of polymers can be piezoelectric. Amorphous polymers are piezo- and pyroelectric by virtue of a non-equilibrium but kinetically stable net dipole orientation in the amorphous phase of the polymer. The semicrystalline polymers are piezoelectric due to alignment of polar, ferroelectric crystals dispersed in the amorphous phase. In both types of polymers, magnitudes of the piezo- and pyroelectric effects are in accord with the expected temperature and pressure dependence of the dipole model. Polarization changes primarily because of dimensional changes of the sample. Space charges embedded in the polymer normally will not produce large piezoelectric and pyroelectric

currents. Those embedded near the crystal-liquid interfaces tend to reduce the piezo- and pyroelectricity. Improved orientation of dipoles and reduction of ionic impurities should increase p_y and d_p for PVDF by a factor of two above typical values presently reported. The sensitivity of amorphous and semicrystalline polymers is limited mainly by dipole moment per unit volume and breakdown strength.

Some of the models presented here were developed along with the writing and were used as a framework for the presentation in order to make the chapter more coherent. It is hoped that these ideas, some largely untested, will provide direction and stimulation for further work in this field.

Acknowledgement

Partial support of this work by the Office of Naval Research is gratefully acknowledged.

TABLE I

Material	d, pC/N		p, nC/cm^{2}K	
Quartz, d_{11}	2.3	(4.134)[a]		
PZT-4, d_{33}	289	(4.135)	27	(4.132)
$BaTio_3$, d_{33}	190	(4.135)	20	(4.132)
Rochelle Salt, d_{25}	53	(4.134)		
Triglycine Sulfate	50	(4.136)	30	(4.132)
$Sr_{0.5}$ $Ba_{0.5}$ Nb_2O_6	95	(4.136)	60	(4.136)
Polyvinylchloride, d_p	0.7	(4.25)	0.1	(4.25)
Polyvinylfluoride	1	(4.6)	1.0	(4.137)
Nylon 11	0.26	(4.138)	.5	(4.138)
Polyvinylidenefluoride, d_{31}	28	(4.13)	4	(4.19)

[a] Numbers in parentheses refer to references at the end of the chapter.

References

4.1 Heaviside, Electrical Papers, Macmillan, London 1, 488 (1892, or Electrical Papers, I. Macmillan, London (1892) p. 488.

4.2 M. Eguchi, Phil. Mag. 49, 178 (1925).

4.3 E. P. Adams, J. Franklin Inst., 204, 469 (1927).

4.4 A. Meissner and R. Bechmann, Z. Tech Phys. 9, 174, and 430 (1928).

4.5 E. Fukada, Progress in Polymer Science, Japan 2, 329 (1971).

4.6 H. Kawai, Jap. J. Appl. Phys. 8, 975 (1969).

4.7 R. Hayakawa and Y. Wada, Advances in Polymer Science, Springer-Verlag, 11, 1 (1973).

4.8 Y. Wada and R. Hayakawa, Japan. J. Appl. Phys. 15, 2041 (1976).

4.9 N. Murayama, J. Polym. Sci., Polym. Phys. Ed., 13, 929 (1975).

4.10 N. Murayama, T. Oikawa, T. Kaito and K. Nakamura, J. Polym. Sci. Polym. Phys. Ed., 13, 1033 (1975).

4.11 N. Tamura, T. Yamaguchi, T. Oyaba and T. Yoshimi, J. Audio Eng. Soc. 23, 21 (1975).

4.12 M. Tamura, K. Ogasawara, N. Ono and S. Hagiwara, J. Appl. Phys. 45, 3768 (1974).

4.13 H. Ohigashi, J. Appl. Phys. 47, 949 (1976).

4.14 J. H. McFee, J. G. Bergman, Jr. and G. R. Crane, Ferroelectrics, 3, 305 (1972).

4.15 J. G. Bergman, G. R. Crane, A. A. Ballman and H. M. O'Bryant, Jr., Appl. Phys. Lett. 21, 497 (1972).

4.16 G. Pfister, M. Abkowitz and R. G. Crystal, J. Appl. Phys. 44, 2064 (1973).

4.17 H. Burkard and G. Pfister, J. Appl. Phys. 45, 3360 (1974).

4.18 M. Abkowitz and G. Pfister, J. Appl. Phys. 46, 2559 (1975).

4.19 G. W. Day, C. A. Hamilton, R. L. Peterson, R. J. Phelan, Jr. and L. O. Mullen, Appl. Phys. Lett. 24, 456 (1974).

4.20 R. L. Peterson, G. W. Day, P. M. Gruzensky and R. J. Phelan, Jr., J. Appl. Phys. 45, 3296 (1974).

4.21 R. G. Kepler and P. M. Beeson, Bulletin APS, Series II, 19, 265 (1974).

4.22 R. G. Kepler, E. J. Graeber and P. M. Beeson, Bulletin APS Series II, 20, 350 (1975).

4.23 D. A. Berlincourt, D. R. Curran and H. Jafee, Physical Acoustics, Academic Press 1A, 183 (1964).

4.24 T. Furukawa and E. Fukada, Rep. Progs. Polym. Phys. Japan, 16, 457 (1973).

4.25 M. G. Broadhurst, W. P. Harris, F. I. Mopsik and C. G. Malmberg, ACS Polymer Preprints 14, 820 (1973).

4.26 R. A. Anderson and R. G. Kepler, Bull. Am. Phys. Soc. 23, 379 (1978).

4.27 J. J. Crosnier, F. Micheron, G. Dreyfus and J. Lewiner, J. Appl. Phys. 47, 4798 (1976).

4.28 T. Ibe, Japan. J. Appl. Phys. 13, 197 (1974).

4.29 R. E. Collins, Rev. Sci. Instrum. 48, 83 (1977).

4.30 A. S. DeReggi, C. M. Guttman, F. I. Mopsik, G. T. Davis and M. G. Broadhurst, Phys. Rev. Lett. 40, 413 (1978).

4.31 P. Laurenceau, G. Dreyfus and J. Lewiner, Phys. Rev. Lett. 38, 46 (1977).

4.32 R. E. Collins, Proceedings of the IEEE, 34, 381 (1973).

4.33 G. M. Sessler and J. E. West, J. Acoust. Soc. Am., 53, 1589 (1973).

4.34 L. Onsager, J. Amer. Chem. Soc. 58, 1486 (1936).

4.35 F. I. Mopsik and M. G. Broadhurst, J. Appl. Phys. 46, 4204 (1975).

4.36 M. Oshiki and E. Fukada, J. Matls. Sci. 10, 1 (1975).

4.37 E. W. Aslaksen, J. Chem. Phys. 57, 2358 (1972).

4.38 K. Iohara, K. Imada and M. Takayanagi, Polym. J. 3, 357 (1972).

4.39 E. Fukada and T. Sakurai, Polym. J. 2, 657 (1971).

4.40 E. Fukada and K. Nishiyama, Japan. J. Appl. Phys. 11, 36 (1972).

4.41 M. G. Broadhurst, C. G. Malmberg, F. I. Mopsik and W. P. Harris in Electrets, Charge Storage and Transport in Dielectrics, M. M. Perlman, Ed. The Electrochemical Soc., NY (1973).

4.42 H. Sussner, Phys. Lett. 58A, 426 (1976).

4.43 G. Natta, I. W. Bassi and G. Allegra, Atti Accad. Nazl. Lincei Rend., Classe Sci. Fis. Mat. Nat. 31, 350 (1961).

4.44 J. Cohen and S. Edelman, J. Appl. Phys. 42, 3072 (1971).

4.45 W. Reddish, J. Polym. Sci., Part C, No. 14, 123 (1966).

4.46 C. E. Wilkes, V. L. Folt and S. Krimm, Macromolecules, 6, 235 (1973).

4.47 A. von Hipple, Dielectric Matls. and Applications (Technology Press of MIT and John Wiley and Sons, NY, 1954).

4.48 G. T. Davis and M. G. Broadhurst in International Symposium on Electrets and Dielectrics, Edited by M. S. deCampos(Academia Brasileira de Cienacias, Rio de Janeiro, 1977)p.299.

4.49 H. G. Olf, Research Triangle Institute, private communication.

4.50 C. W. Wilson, III and E. R. Santes, Jr., J. Polym. Sci., Pt. C, 8, 97 (1965).

4.51 M. Gorlitz, R. Minke, W. Trautvetter and G. Weisgerber, Die Angewandte Makromolekulare Chemie 29/30, 137 (1973).

4.52 J. P. Stallings and S. G. Howell, Polymer Eng. & Sci. 11, 507 (1971).

4.53 W. M. Prest, Jr. and D. J. Luca, J. Appl. Phys. 46, 4136 (1975).

4.54 W. M. Prest, Jr. and D. J. Luca, to be published in J. Appl. Phys. Oct. 1978.

4.55 S. Osaki and Y. Ishida, J. Polym. Sci., Polym. Phys. Ed. 13, 1071 (1975).

4.56 R. J. Shuford, A. F. Wilde, J. J. Ricca and G. R. Thomas, Polym. Eng. Sci. 16, 25 (1976).

4.57 J. B. Lando, H. G. Olf and A. Peterlin, J. Polym. Sci. A-1, 4, 941 (1966).

4.58 K. Nakagawa and Y. Ishida, J. Polym. Sci., Polym. Phys. Ed. 11, 2153 (1973).

4.59 J. P. Reardon and P. F. Waters, in Thermal and Photostimulated Currents in Insulators. D. M. Smyth, ed. Electrochem. Soc., Princeton, NJ, p. 185 (1976).

4.60 N. Sasabe, S. Saito, M. Asahina and H. Kakutani, J. Polym. Sci. A-2, 7, 1405 (1969).

4.61 S. Osaki and Y. Ishida, J. Polym. Sci., Polym. Phys. Ed., 12, 1727 (1974).

4.62 H. Kakutani, J. Polym. Sci. A-2, 8, 1177 (1970).

4.63 M. Blukis, C. Lewa, S. Letowski and A. Sliwinski, Ultrasonics Int'l. __, 474 (1977).

4.64 E. Fukada and K. Nishiyama, Japanese J. Appl. Phys. 11, 36 (1972).

4.65 M. E. Baird, P. Blackburn and B. W. Delf, J. Matls. Sci. 10, 1248 (1975).

4.66 G. R. Davies, A. Killey, A. Pushworth and H. Singh, Organic Coatings and Plastics Chemistry, 38, 257 (1978) [Preprints for ACS meeting in Anaheim, CA, Mar. 1978].

4.67 E. L. Galperin, Yu. V. Strogalin, and M. P. Mlenik, Vysokomol. Soedin. 7, 933 (1965).

4.68 W. M. Doll and J. B. Lando, J. Macromol. Sci.-Phys., B4, 309 (1970).

4.69 M. Kobayashi, K. Tashiro and H. Tadokoro, Macromolecules, 8, 159 (1975).

4.70 S. Osaki and Y. Ishida, J. Polymer Sci., Polym. Phys. Ed., 13, 1071 (1975).

4.71 R. Hasegawa, Y. Tanabe, M. Kobayashi, H. Tadokoro, A. Sawaoka and N. Kawai, J. Polym. Sci., A-2, 8, 1073 (1970).

4.72 R. Hasegawa, Y. Takahashi, Y. Chatani and H. Tadokoro, Polymer J. 3, 600 (1972).

4.73 J. B. Lando, M. H. Litt and S. Weinhold, Case Western Reserve Univ., private communication.

4.74 G. Natta, G. Allegra, I. W. Bassi, D. Sianese, G. Copoucci and E. Torti, J. Polym. Sci. A, 3, 4263 (1965).

4.75 B. L. Farmer, A. J. Hopfinger and J. B. Lando, J. Appl. Phys. 43, 4293 (1972).

4.76 R. D. Nelson, Jr., D. R. Lide, Jr. and A. A. Maryott, Selected Values of Electric Dipole Moments for Molecules in the Gas Phase, NSRDS-NBSIO, U. S. Government Printing Office, Washington, D.C. (1967).

4.77 G. T. Davis, J. E. McKinney, M. G. Broadhurst and S. C. Roth, to be published in J. Appl. Phys., Oct. 1978.

4.78 K. Nakagawa and Y. Ishida, J. Polym. Sci. A-2, 11, 1503 (1973).

4.79 L. E. Alexander, X-ray Diffraction Methods in Polymer Science, John Wiley, NY (1969).

4.80 S. Osaki, S. Uemura and Y. Ishida, J. Polym. Sci. A-2, 9, 585 (1971).

4.81 A. Peterlin and J. Elwell, J. Matls. Sci. 2, 1 (1967).

4.82 S. Yano, J. Polym. Sci. A-2, 8, 1057 (1970).

4.83 S. Yano, K. Tadano, K. Aoki, and N. Koizumi, J. Polym. Sci., Polym. Phys. Ed., 12, 1875 (1974).

4.84 N. Murayama and H. Hashizume, J. Polym. Sci., Polym. Phys. Ed., 14, 999 (1976).

4.85 G. R. Davies and A. Killey, University of Leeds, private communication from thesis of A. Killey.

4.86 J. D. Hoffman, G. Williams and E. Passaglia, J. Polym. Sci., C, No. 14, 173 (1966).

4.87 Y. Miyamoto, H. Miyaji and K. Asai, Reports on Prog. Polym. Phys. Japan, 20, 371 (1977).

4.88 M. G. Broadhurst, to be published.

4.89 P. Weiss, J. Physique 6, 661 (1907).

4.90 W. L. Bragg and E. J. Williams, Proc. Roy. Soc. A145, 699 (1934).

4.91 W. P. Mason, Phys. Rev. 72, 854 (1947).

4.92 H. Fröhlich, Theory of Dielectrics, Oxford University Press, London (1949).

4.93 P. Buchman, Ferroelectrics, 5, 39 (1973).

4.94 M. Kobayashi, K. Tashiro and H. Tadokoro, Macromolecules, 8, 163 (1975).

4.95 M. G. Broadhurst and F. I. Mopsik, J. Chem. Phys. 52, 3634 (1970).

4.96 K. Nakamura and Y. Wada, J. Polym. Sci., A-2, 9, 161 (1971).

4.97 J. H. McFee, J. G. Bergman, Jr. and G. R. Crane, Ferroelectrics, 3, 305 (1972).

4.98 R. G. Kepler and R. A. Anderson, J. Appl. Phys. 49,1232 (1978).

4.99 G. L. Cessac and J. G. Curro, J. Polym. Sci., Polym. Phys. Ed., 12, 695 (1974).

4.100 R. G. Kepler, Organic Coatings and Plastics Chemistry, 38, 278 (1978) (Preprints for ACS Meeting in Anaheim, CA, March 1978).

4.101 J. C. Hicks, T. E. Jones and J. C. Logan, to be published.

4.102 E. Fukada, M. Date and T. Furukawa, Organic Coatings and Plastics Chemistry, 38, 262 (1978) [Preprints for ACS Meeting in Anaheim, CA, March 1978].

4.103 D. Maegele and D. Y. Yoon, to be published in Appl. Phys. Lett. (1978).

4.104 J. P. Luongo, J. Polym. Sci. A-2 10, 1119 (1972).

4.105 J. E. McKinney and G. T. Davis, Organic Coatings and Plastics Chemistry, 38, Preprints of papers for 175th meeting of ACS in Anaheim, CA, March 1978, p. 271.

4.106 D. K. Das Gupta and K. Doughty, Appl. Phys. Lett. 31. 585 (1977).

4.107 D. K. Das Gupta and K. Doughty, J. Appl. Phys. 49, 4601 (1978).

4.108 P. D. Southgate, Appl. Phys. Lett. 28, 250 (1976).

4.109 M. Tamura, S. Hagiwara, S. Matsumoto and N. Ono, J. Appl. Phys. 48, 513 (1977).

4.110 H. Sussner and K. Dransfeld, J. Polym. Sci., Polym. Phys. Ed., 16, 529 (1978).

4.111 J. van Turnhout, Polym. J. 2, 173 (1971).

4.112 E. C. Cassidy, R. E. Hebner, Jr., M. Zahn and R. J. Sojka, IEEE Trans. on Elec. Insulation, 9, 43 (1974).

4.113 S. Uemura, J. Polym. Sci., Polym. Phys. Ed., 10, 2155 (1972).

4.114 J. M. Kenney, National Bureau of Standards, private communication.

4.115 T. Hanai, Kolloid-Zeitschrift, 171, 23 (1960).

4.116 A. K. Vijh, J. Appl. Phys. 49, 3621 (1978).

4.117 A. I. Baise, H. Lee, B. Oh, R. E. Salomon and M. M. Labes, Appl. Phys. Lett. 26, 428 (1975).

4.118 H. Sussner and D. Y. Yoon, Organic Coatings and Plastics Chemistry, 38, 331 (1978) [Preprints for ACS Meeting in Anaheim, CA, March 1978].

4.119 T. Hanai, N. Koizumi, T. Saigano and R. Gotoh, Kolloid-Zeitschrift, 171, 20 (1960).

4.120 J. Van Turnhout, Thesis Leiden (1972), TNO Central Laboratorium Communication, No. 471.

4.121 Y. Sakamoto, H. Fukagawa, T. Shikama, K. Kimura and H. Takehana, Fujikura Tech. Review, p. 22 (1977).

4.122 P. E. Bloomfield, I. Lefkowitz and A. D. Aronoff, Phys. Rev. B4, 974 (1971).

4.123 R. J. Phelan, Jr., R. L. Peterson, C. A. Hamilton and G. W. Day, Ferroelectrics, 7, 375 (1974).

4.124 C. B. Duke and T. J. Fabish, J. Appl. Phys. 49, 315 (1978).

4.125 D. K. Davies, Brit. J. Appl. Phys. (J. Phys. D) 2, 1533 (1969).

4.126 D. K. Davies, J. Phys. D: Appl. Phys. 5, 1017 (1973).

4.127 A. W. Stephens, A. W. Levine, J. Fech, Jr., T. J. Zrebiec, A. V. Cafiero and A. M. Garofalo, Thin Solid Films, 24, 362 (1974).

4.128 H. Sussner, D. E. Horne and D. Y. Yoon, Bull. Am. Phys. Soc. 23, 370 (1978).

4.129 W. R. Blevin, Appl. Phys. Lett. 31, 6 (1977).

4.130 E. Fukada and M. Oshiki, Nat. Bur. Stand. (U.S.) Interagency Rep. 75-760, pgs. 9-34 (1975).

4.131 N. Murayama, K. Nakamura, H. Obara and M. Segewa, Ultrasonics 14, 15 (1976).

4.132 L. E. Garn and E. J. Sharp, IEEE Trans, in Parts, Hybrids and Packaging, PHP10, 28 (1974).

4.133 K. Takahashi, R. E. Salomon and M. M. Labes, Bull. Am. Phys. Soc. 23, 378 (1978).

4.134 W. G. Cady, Piezoelectricity, McGraw Hill, NY (1946).

4.135 D. A. Berlincourt, D. R. Curran and H. Jaffe, Chapter 3 in Physical Acoustics, Vol. 1, part A, Academic Press, NY (1964).

4.136 S. T. Liu and D. Long, Proc. I.E.E.E. 66, 14, (1978).

4.137 R. J. Phelan, Jr., R. J. Mahler and A. R. Cook, Appl. Phys. Lett. 19, 337 (1971).

4.138 M. H. Litt, C. Hsu, and P. Basu, Tech. Report No. 5 on Office of Naval Research Contract No. N000 14-75-C-0842.

4.139 W. R. Blevin and J. Geist, Appl. Opt. 13, 2212 (1974).

4.140 J. Stern and S. Edelman, Nat'l. Bur. of Stds. (U.S.) Technical News Bulletin, 56, No. 3, 52 (1972).

4.141 J. M. Powers, Nat'l. Bur. Stds. (U.S.) Interagency Rep. 75-760, pg. 209 (1975).

4.142 M. Jacobs, NBS Dimensions, 62 (2), 2 (1978); U.S. Dept. of Commerce.

4.143 A. L. Robinson, Science 200, 1371 (1978).

4.144 Materials Engineering, p. 6, May 1978.

4.145 M. G. Broadhurst, G. T. Davis, J. E. McKinney and P. E. Collins, to be published in J. Appl. Phys., Oct. 1978.

4.146 e/K. N. Nakagawa and Y. I. Ishida, Kolloid Z. Z. Polymere, 251, 103 (1973).

4.147 B. A. Newman, C. H. Yoon and K. D. Pae, Technical Report No. 11 under Office of Naval Research Contract N00014-75-C-0540.

4.148 W. W. Doll and J. B. Lando, J. Macromol. Sci. Phys. B2, 219 (1968).

4.149 K. Nakagawa and Y. Ishida, J. Polym. Sci., Polym. Phys. Ed., 11, 2153 (1973).

4.150 R. G. Kepler and R. A. Anderson, J. Appl. Phys. 49, 4490 (1978).

4.151 D. Berlincourt and H. H. A. Krueger, J. Appl. Phys. 30, 1804 (1959).

4.152 B. A. Newman, Rutgers University, private communication.

4.153 R. G. Kepler and R. A. Anderson, J. Appl. Phys. 49, 4918 (1978).

4.154 R. Hayakawa, J. Kusuhara, K. Hattori and Y. Wada, Repts. Prog. Polym.

4.155 R. E. Salomon and M. M. Labes, Nat'l. Bur. Stds. (U.S. Interagency Rep. 75-760, pg. 199-209 (1975).

Figure Captions

Figure 4.1 A diagram of poling procedure showing the temperature T, voltage Φ, time t sequence and the resulting polarization P reduced by the permittivity of free space ε_o and applied field E_p, The remaining frozen-in reduced polarization is the difference between relative permittivities ε' at the two temperatures T_r and T_g.

Figure 4.2 A model of an electret with real charges and preferentially ordered dipolar charges resulting from the applied voltage Φ.

Figure 4.3 A model of an electret with a sheet of real charge embedded in it and induced charges on the short circuited electrodes. The σ are the surface charge densities located at the various positions, o, x and s.

Figure 4.4 Schematic diagram showing the principles of an electret microphone.

Figure 4.5 A model of a dipolar electret showing the flow of charge resulting from a thickness change due to an increase in pressure or a decrease in temperature.

Figure 4.6 A model showing how the electret of Fig. 4.5 is used for a pyroelectric application. Note the interaction of the film with the radiation takes place in the electrode which in turn acts as a heat bath.

Figure 4.7 A model for an electret containing a representative dipole of moment μ_o, polarizability α, and fixed mean orientation θ with respect to the net polarization P.

Figure 4.8 A model showing the decrease in the mean moment of a librating dipole with a temperature-induced increase in the libration amplitude.

Figure 4.9 The identification of axes for a stretched and poled polymer specimen.

Figure 4.10 Pyroelectric coefficient as a function of poling field for the amorphous polymer, PVC, and the semicrystalline polymer, PVDF. PVC data are from reference 4.48, PVDF data are from reference 4.19 (Δ) and unpublished data of J. M. Kenney, N.B.S. (o).

Figure 4.11 Schematic diagram illustrating essential features of spherulitic morphology in semi-crystalline polymers such as PVF and PVDF. Molecular chain axes are approximately normal to the surfaces of the lamellar platelets which grow radially from the center of the structure.

Figure 4.12 Projections on a plane normal to the molecular axes of the α and β crystal forms of PVDF. Large circles represent fluorine atoms, small circles represent carbon atoms and hydrogen atoms are omitted.

Figure 4.13 Potential energy diagram for a two site model in which a molecular dipole becomes reoriented with respect to its neighbors under the influence of an electric field.

Figure 4.14 The ratio of the average moment to the actual moment per dipole in the two site model of Fig. 4.13 as a function of the electric field to which it is subjected. Curves are drawn for different values of the energy difference between sites for the perfectly ordered system. The dashed lines correspond to a ferroelectric hysteresis loop for an ideal crystal.

Figure 4.15 Calculated equilibrium Helmholtz free energy of partially ordered system of dipoles relative to the completely disordered system as a function of the ratio of the average moment to the actual moment per dipole. Curves are drawn for different values of the energy difference between sites as in Fig. 4.14 in the absence of an applied field ($E=0$)

Figure 4.16 Calculated Helmholtz free energy of a partially ordered system of dipoles as a function of the ratio of the average moment to the actual moment per molecule. Curves are drawn for different values of an externally applied field and apply to the case when $U_o/kT = 1.5$.

Figure 4.17 Schematic diagram of interfacial polarization in a semicrystalline polymer in an applied dc field due to charge build up at crystalline obstructions.

Figure 4.18 A schematic diagram illustrating dipole alignment within a polar crystal and possible counter charge at the crystal liquid interface. A typical active polymer film consists of an array of such objects with a preferential dipole alignment resulting from the poling procedure.

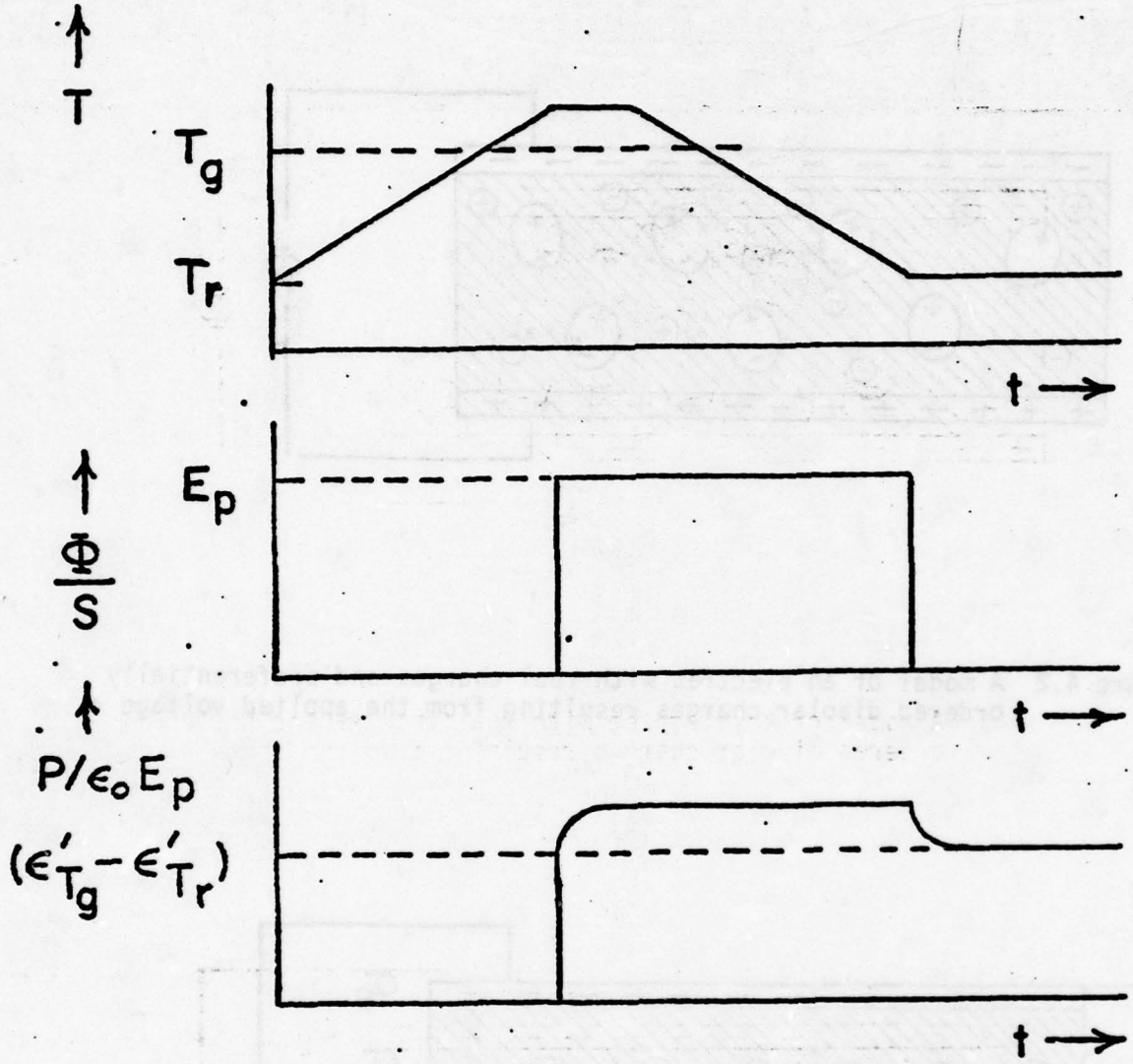

Figure 4.1 A diagram of poling procedure showing the temperature T, voltage Φ, time t sequence and the resulting polarization p reduced by the permittivity of free space ϵ_o and applied field E_p. The remaining frozen-in reduced polarization is the difference between relative permittivities ϵ' at the two temperatures T_r and T_g.

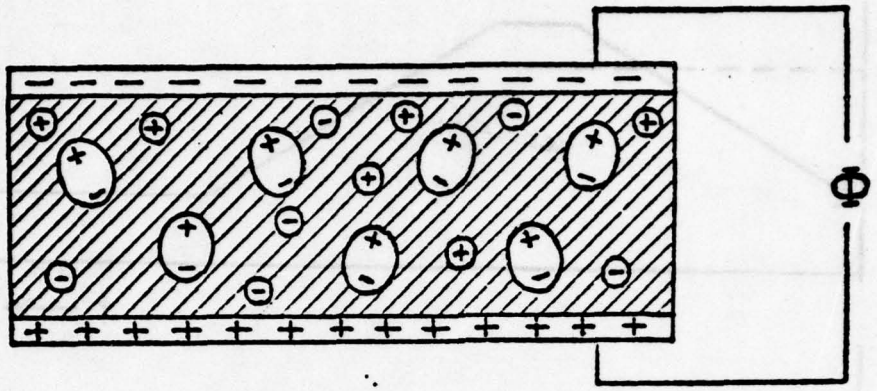

Figure 4.2 A model of an electret with real charges and preferentially ordered dipolar charges resulting from the applied voltage Φ.

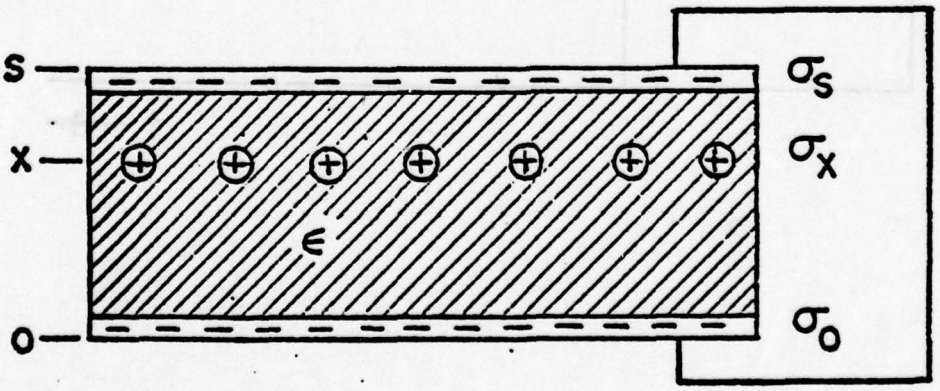

Figure 4.3 A model of an electret with a sheet of real charge embedded in it and induced charges on the short circuited electrodes. The σ are the surface charge densities located at the various positions, o, x and s..

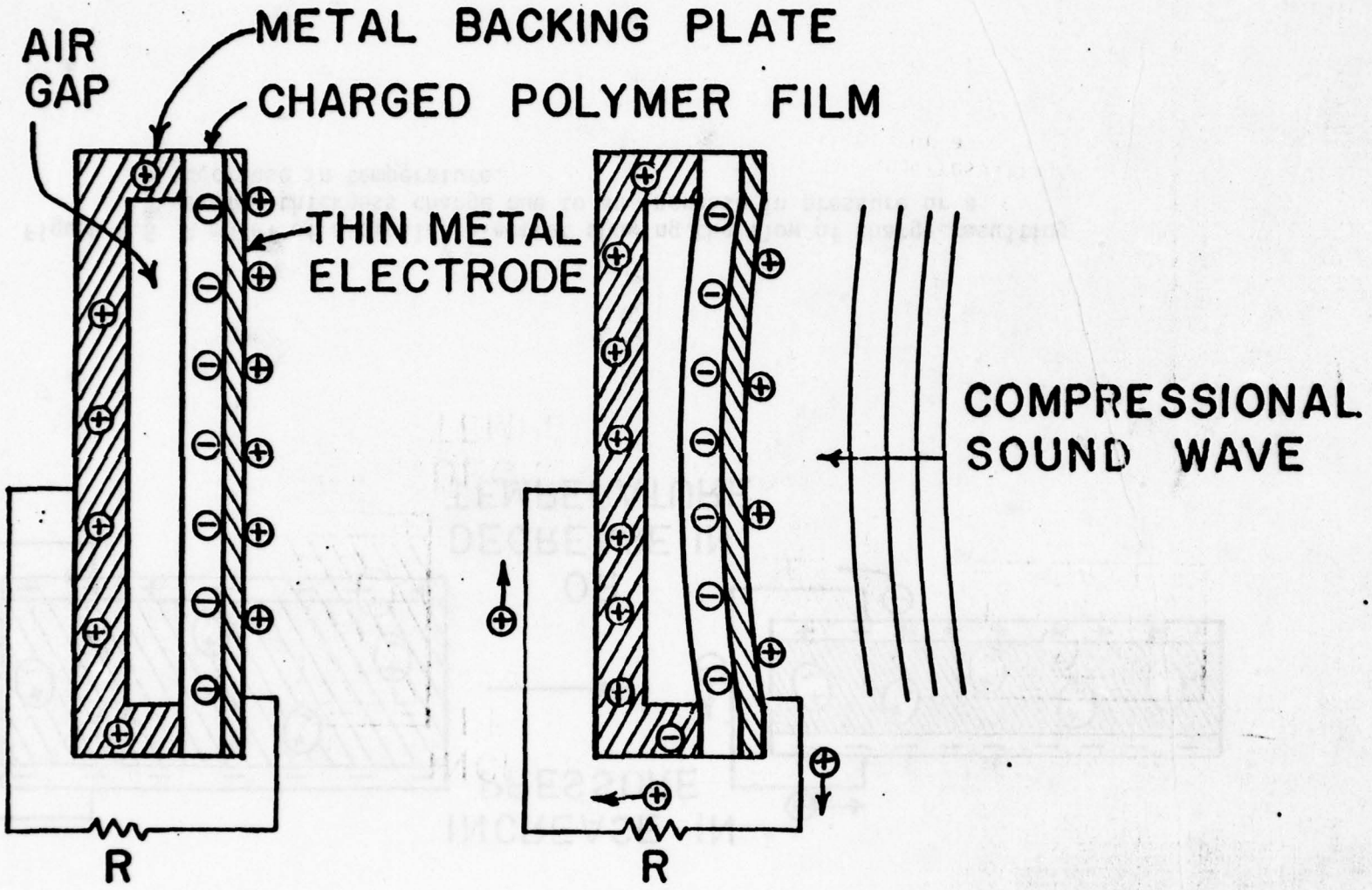

Figure 4.4 Schematic diagram showing the principles of an electret microphone.

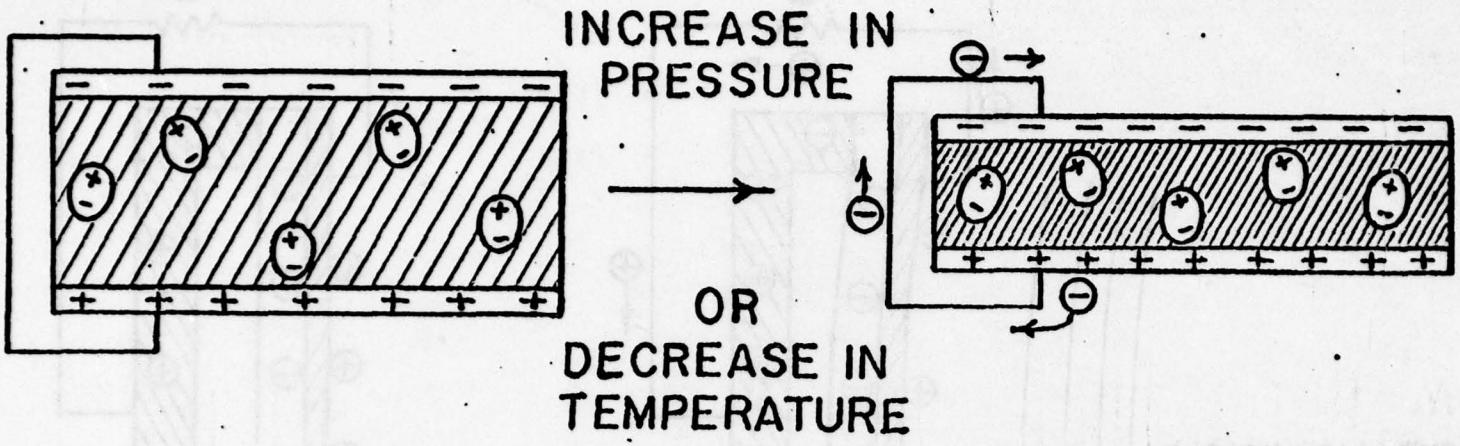

Figure 4.5 A model of a dipolar electret showing the flow of charge resulting from a thickness change due to an increase in pressure or a decrease in temperature.

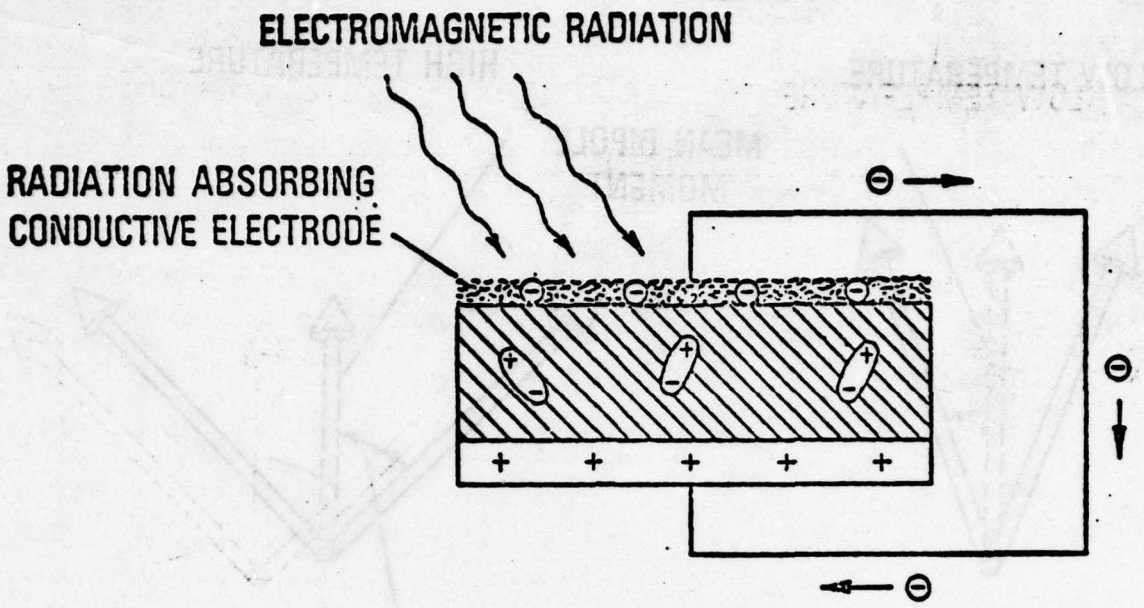

Figure 4.6 A model showing how the electret of Fig. 4.5 is used for a pyroelectric application. Note the interaction of the film with the radiation takes place in the electrode which in turn acts as a heat bath.

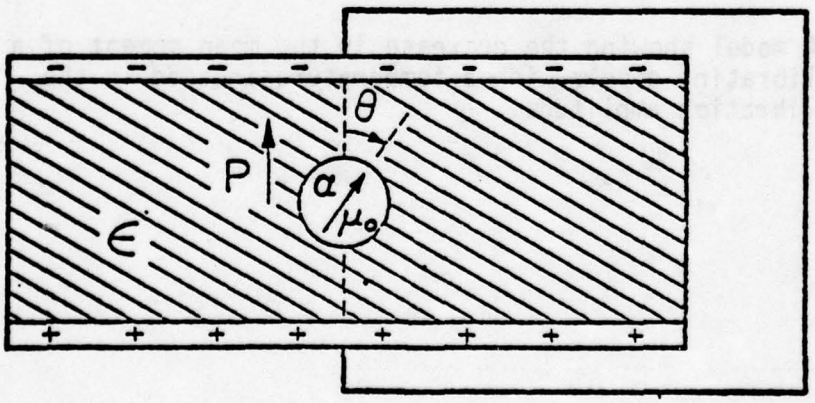

Figure 4.7 A model for an electret containing a representative dipole of moment μ_o, polarizability α and fixed mean orientation θ with respect to the net polarization P.

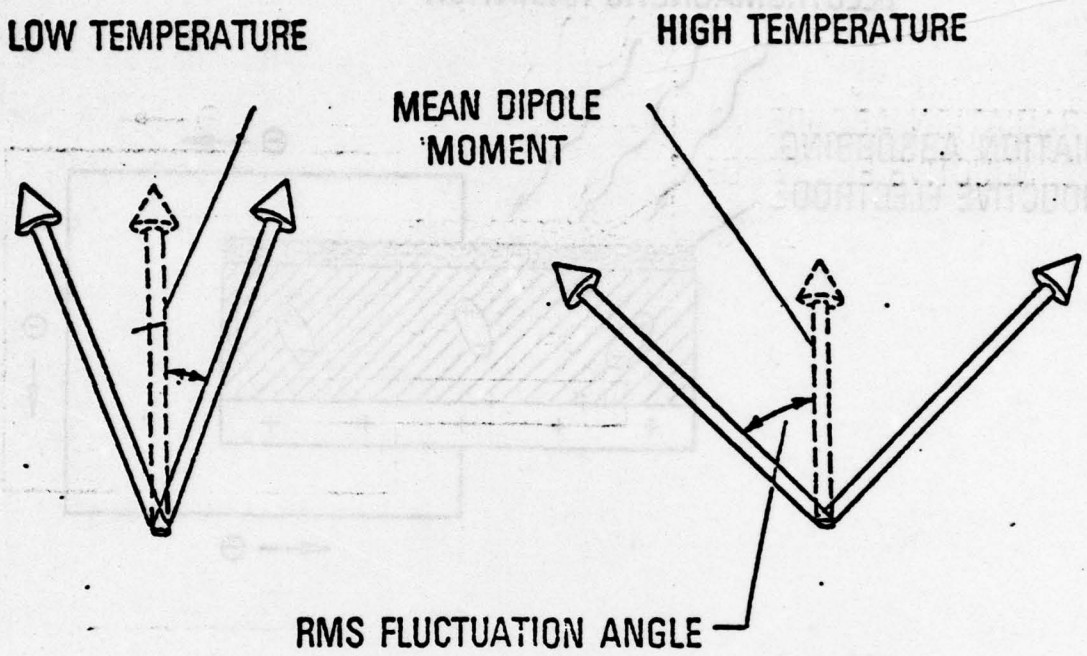

Figure 4.8 A model showing the decrease in the mean moment of a librating dipole with a temperature-induced in the libration amplitude.

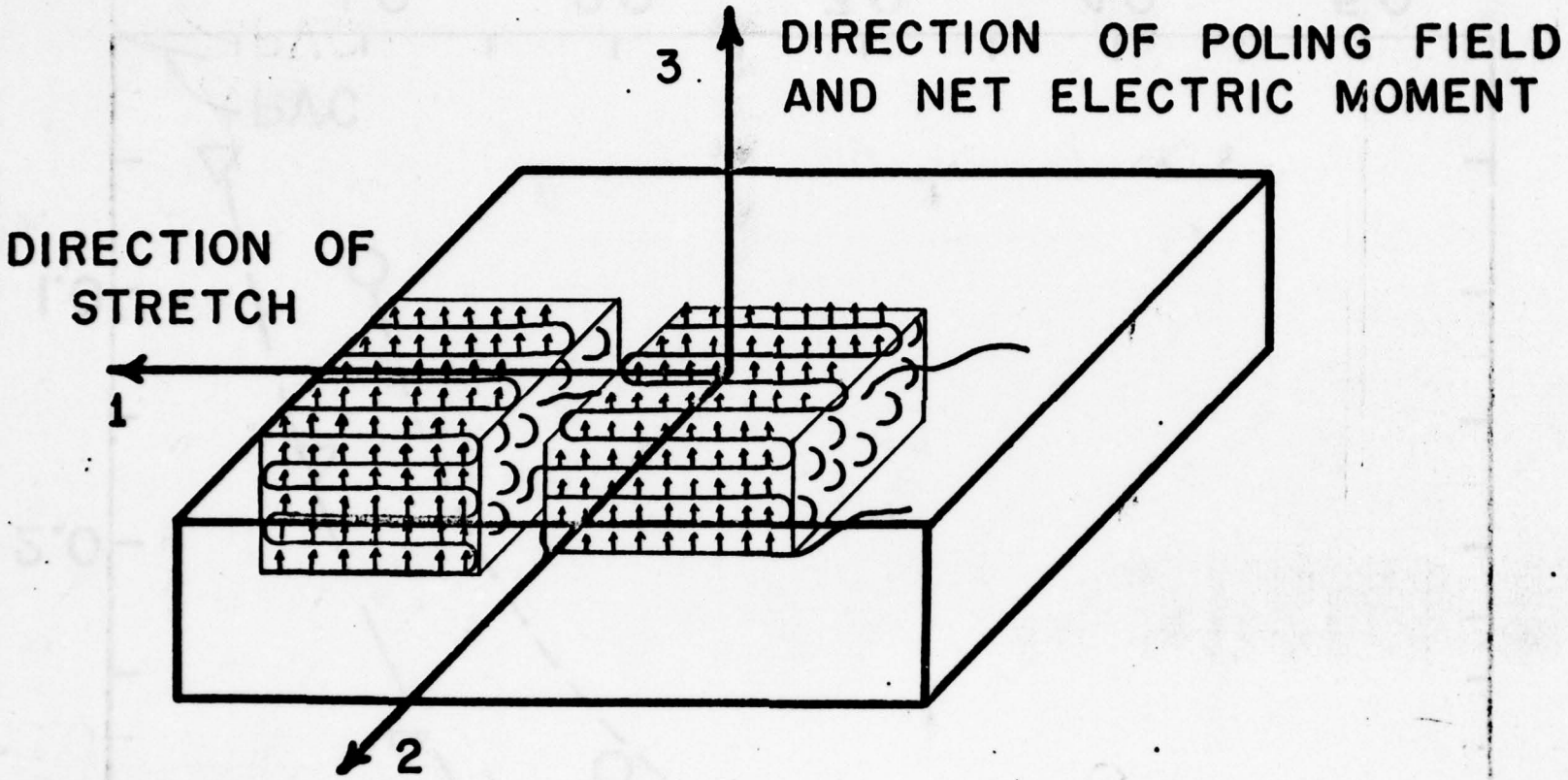

Figure 4.9 The identification of axes for a stretched and poled polymer specimen.

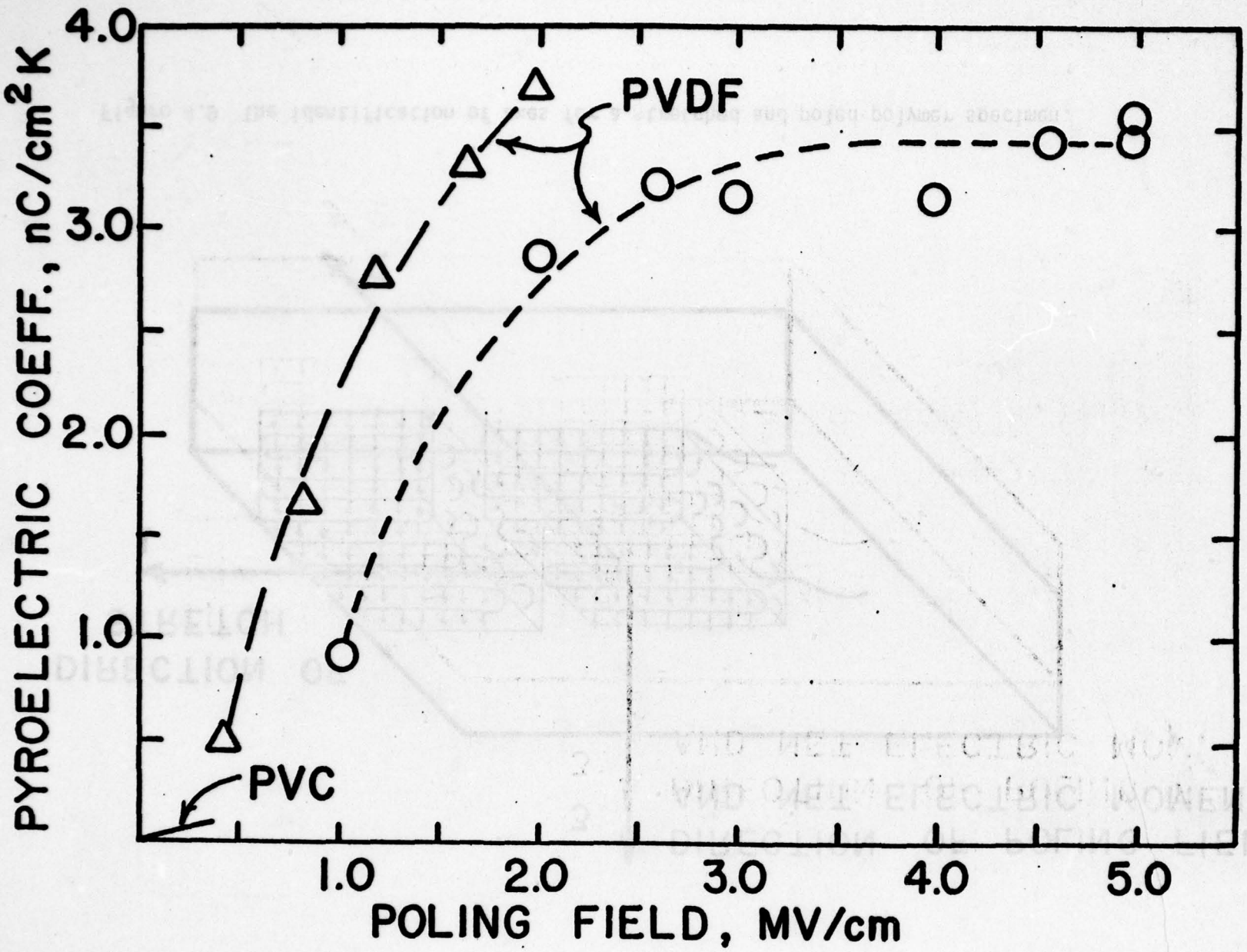

Figure 4.10 Pyroelectric coefficient as a function of poling field for the amorphous polymer, PVC, and the semicrystalline polymer, PVDF. PVC data are from reference 4.48, PVDF data are from reference 4.19 (Δ) and unpublished data of J. M. Kenney, NBS (o).

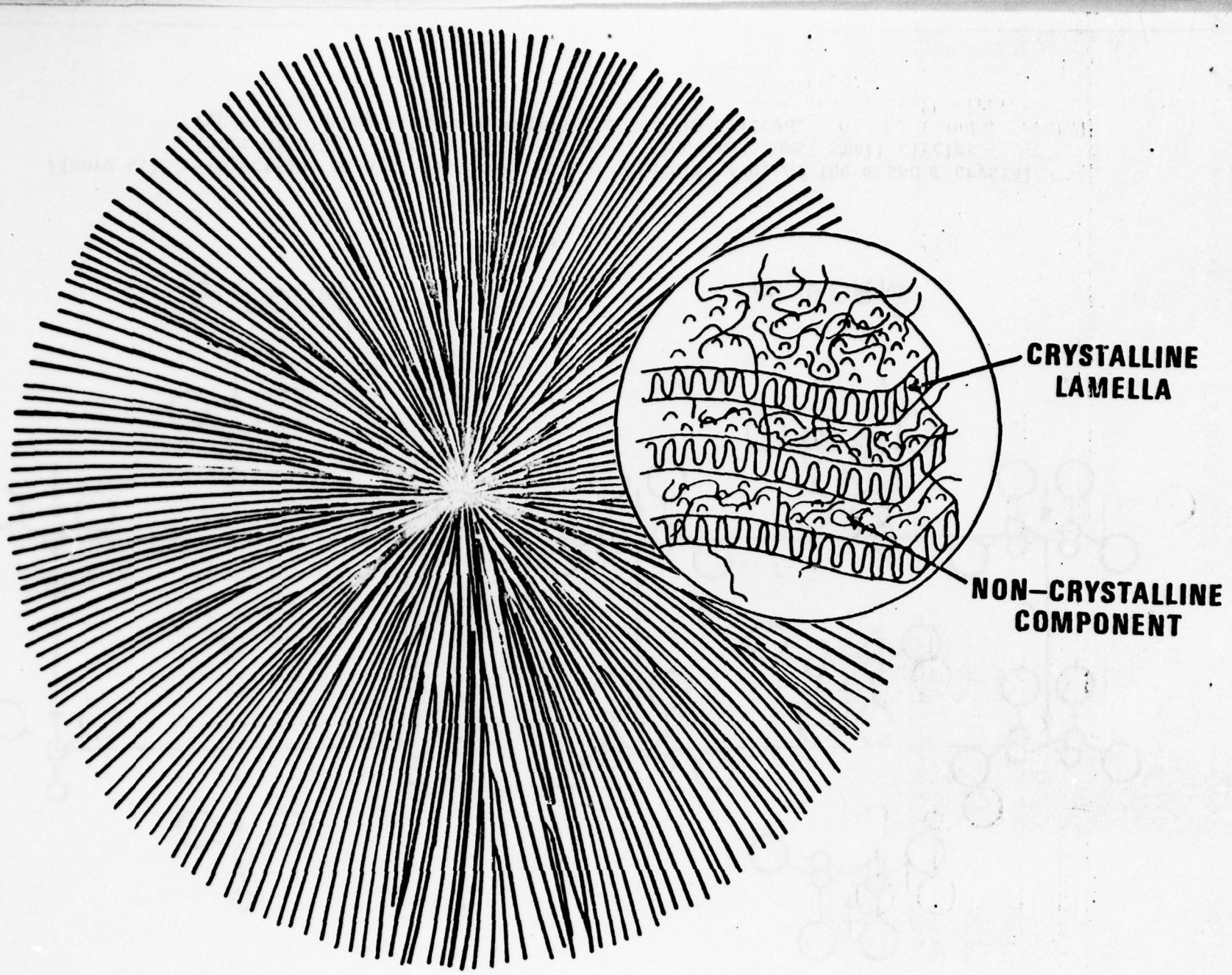

Figure 4.11 Schematic diagram illustrating essential features of spherulitic morphology in semi-crystalline polymers such as PVF and PVDF. Molecular chain axes are approximately normal to the surfaces of the lamellar platelets which grow radially from the center of the structure.

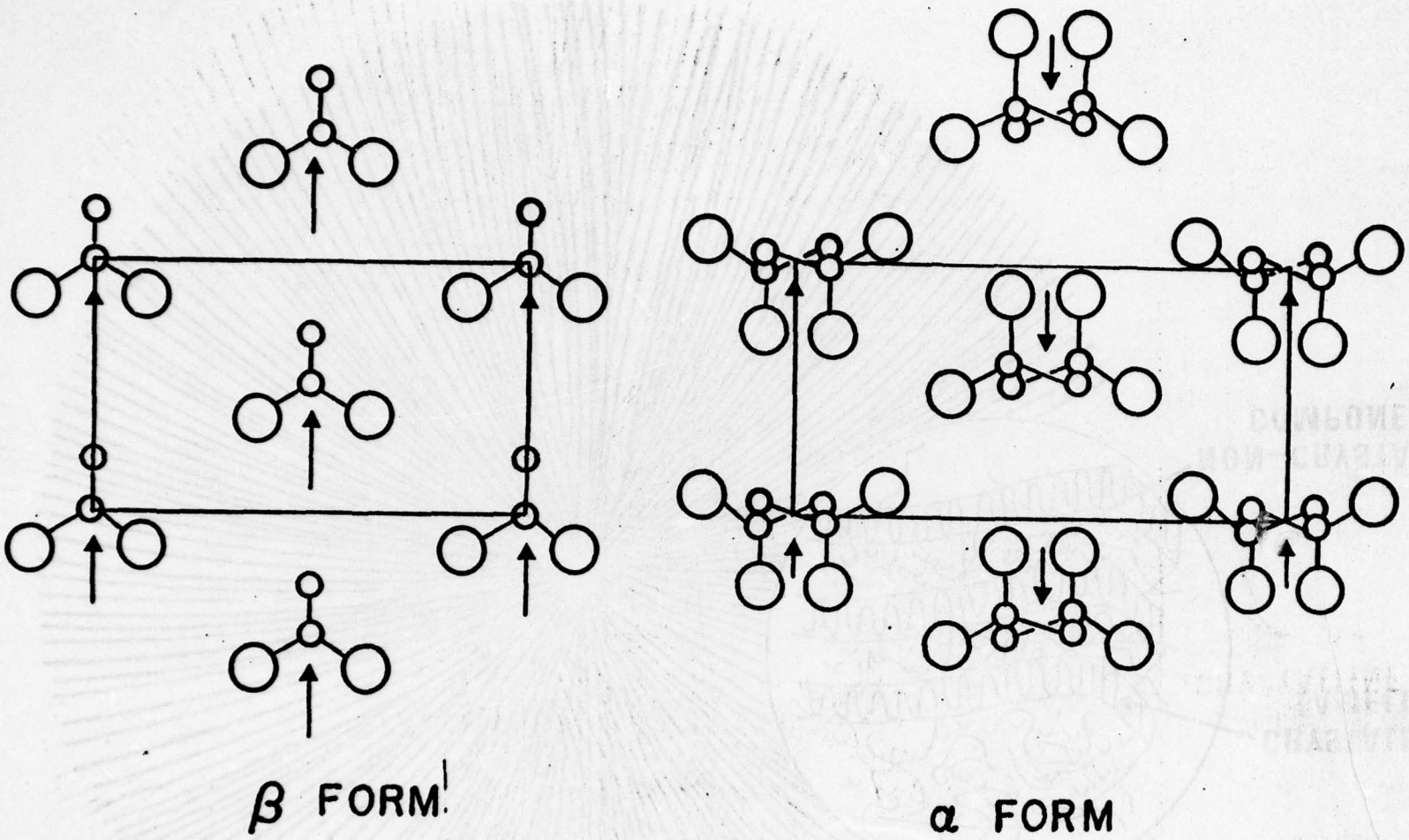

Figure 4.12 Projections on a plane normal to the molecular axes of the α and β crystal forms of PVDF. Large circles represent fluorine atoms, small circles represent carbon atoms and hydrogen atoms are omitted.

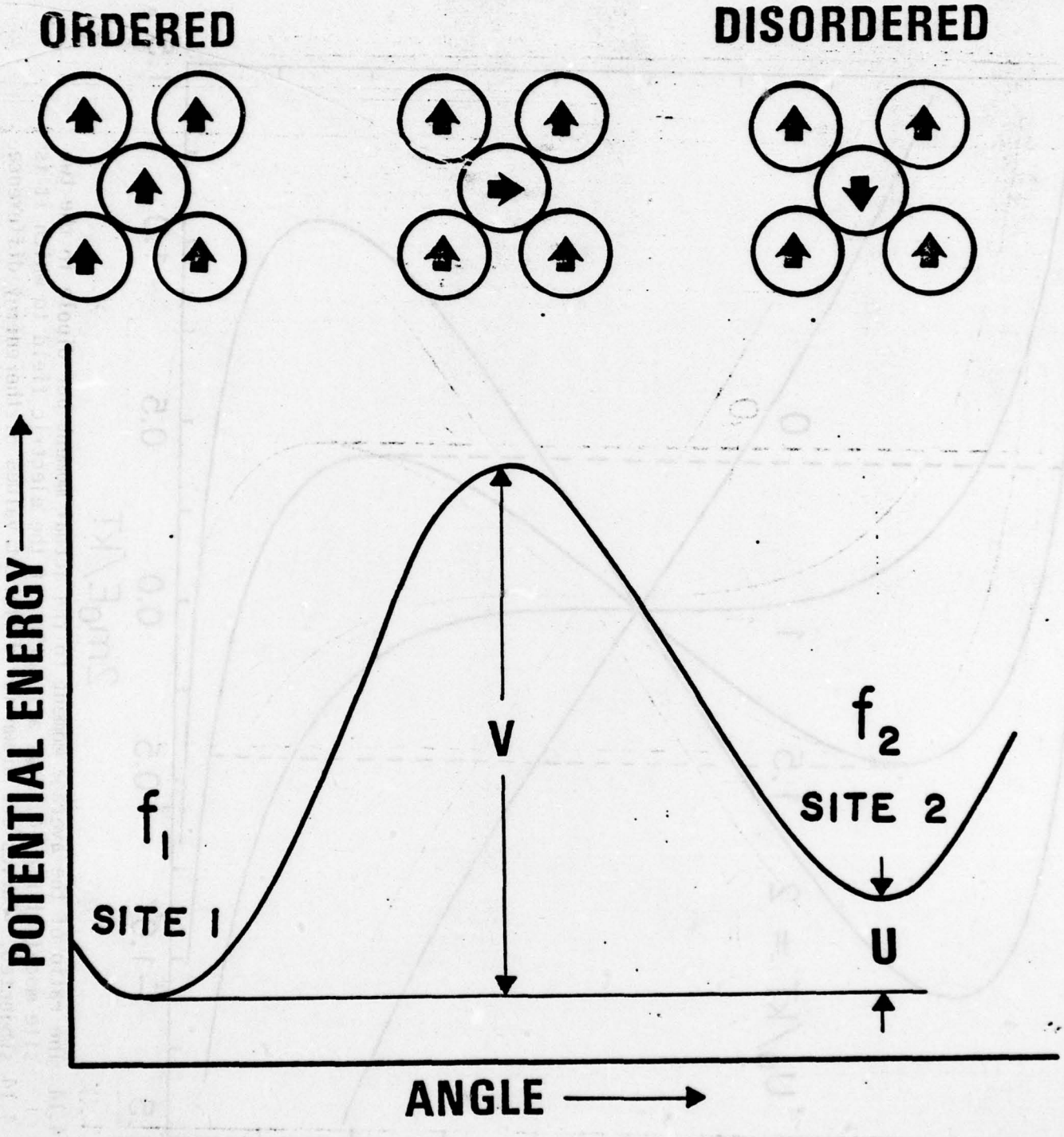

Figure 4.13 Potential energy diagram for a two site model in which a molecular dipole becomes reoriented with respect to its neighbors under the influence of an electric field.

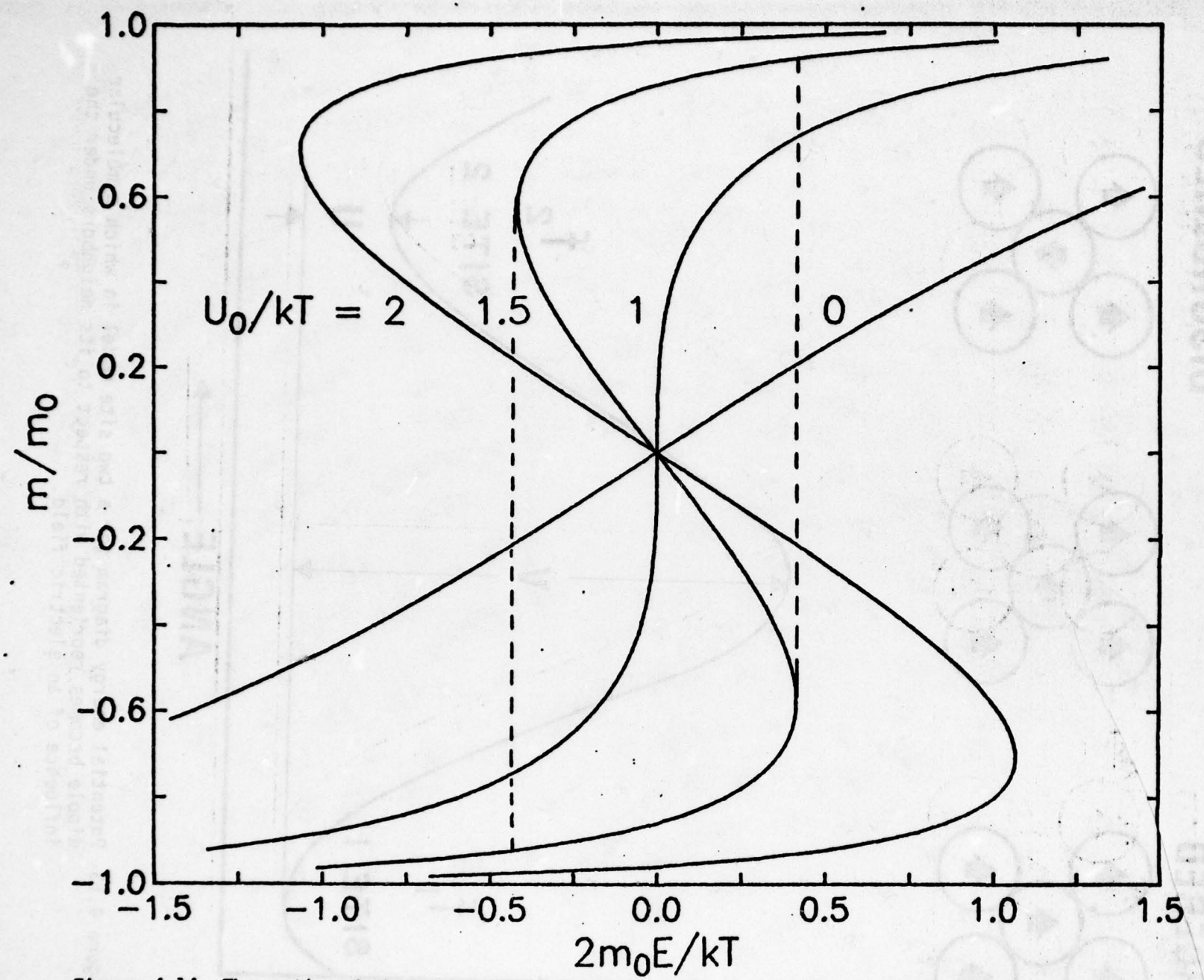

Figure 4.14 The ratio of the average moment to the actual moment per dipole in the two site model of Fig. 4.13 as a function of the electric field to which it is subjected. Curves are drawn for different values of the energy difference between sites for the perfectly ordered system. The dashed lines correspond to a ferroelectric hysteresis loop for an ideal crystal.

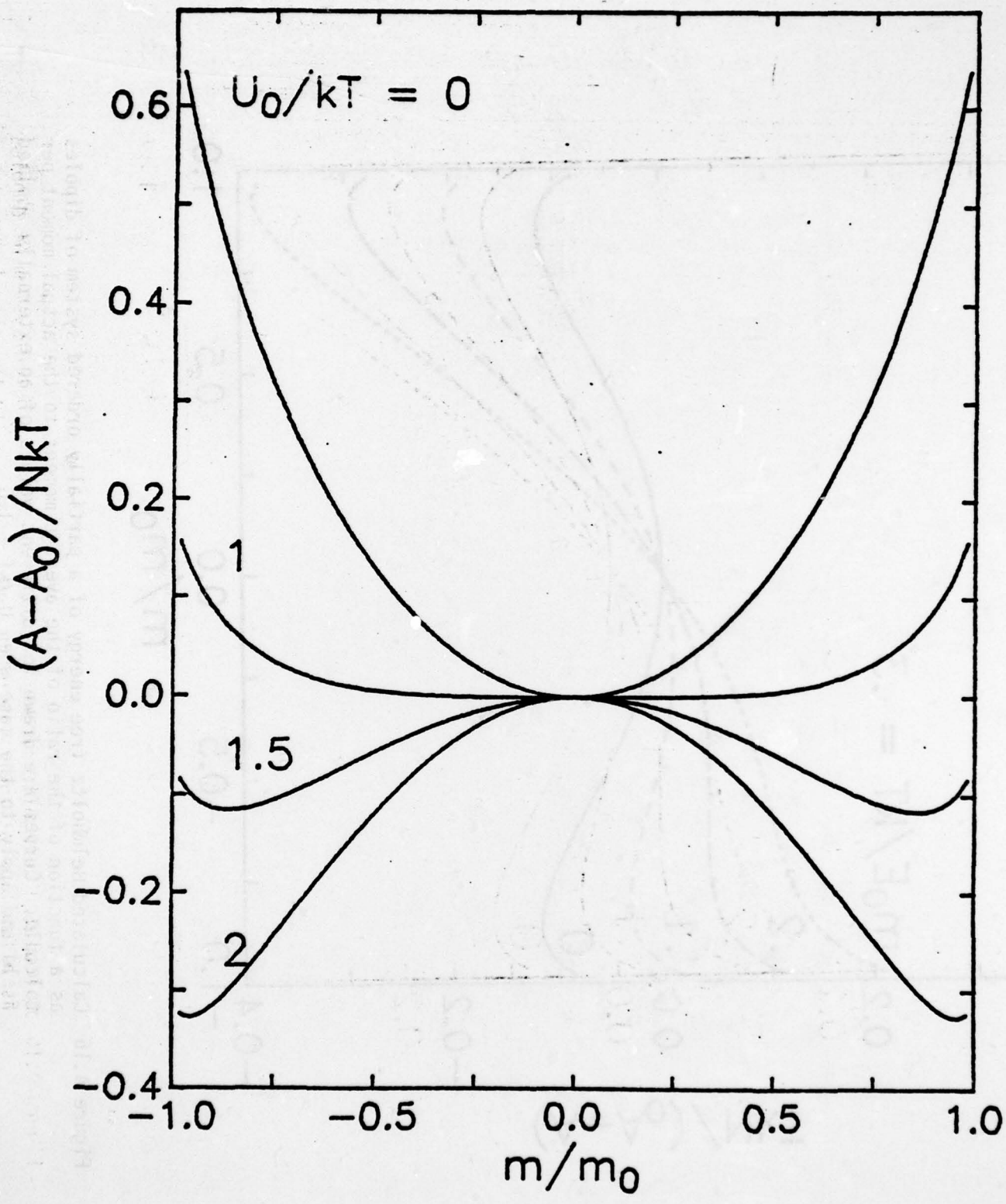

Figure 4.15 Calculated equilibrium Helmholtz free energy of partially ordered system of dipoles relative to the completely disordered system as a function of the ratio of the average moment to the actual moment per dipole. Curves are drawn for different values of the energy difference between sites as in Fig. 4.14 in the absence of an apolied field (E=0)

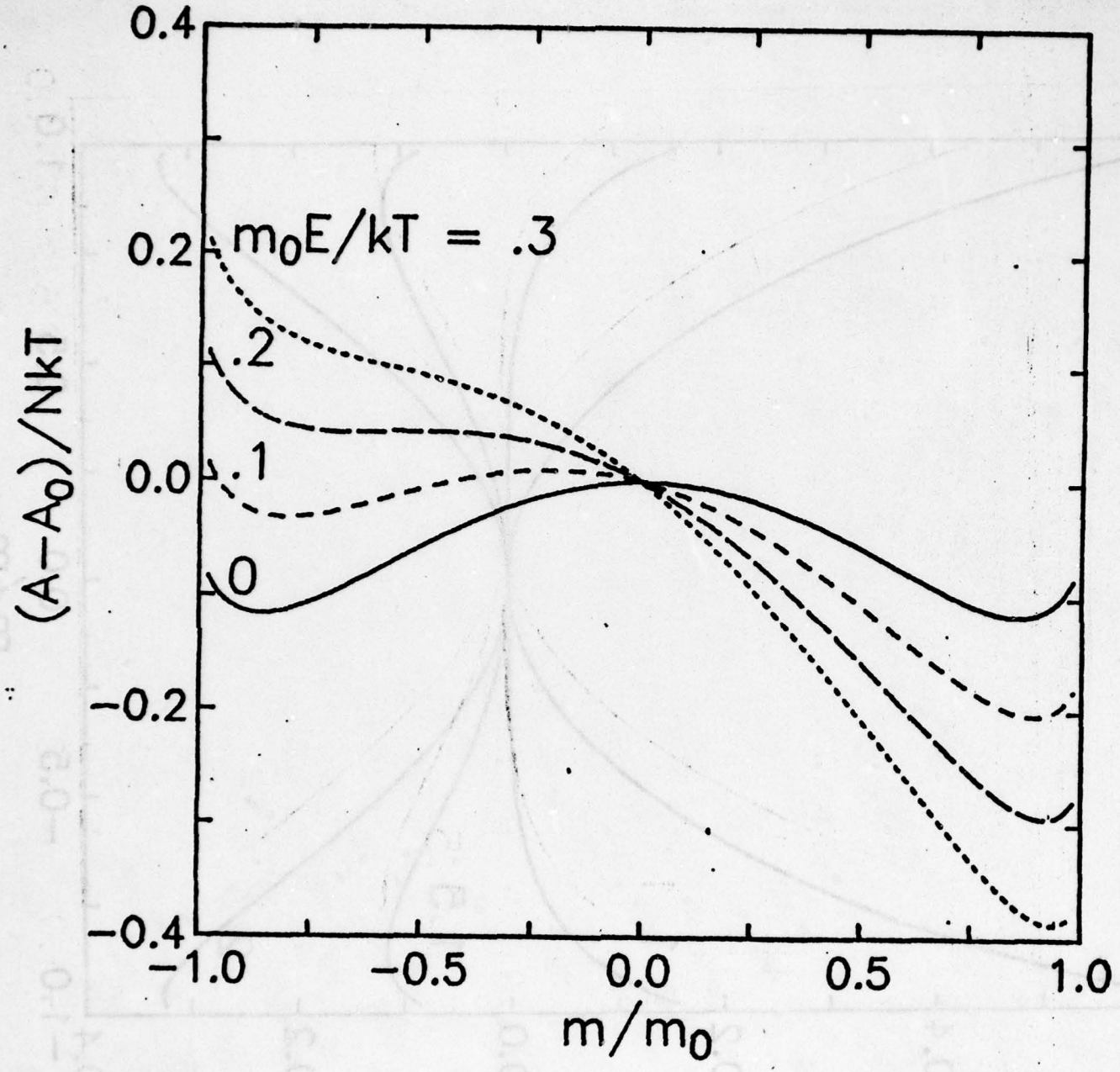

Figure 4.16 Calculated Helmholtz free energy of a partially ordered system of dipoles as a function of the ratio of the average moment to the actual moment per molecule. Curves are drawn for different values of an externally applied field and apply to the case when $U_0/kT = 1.5$

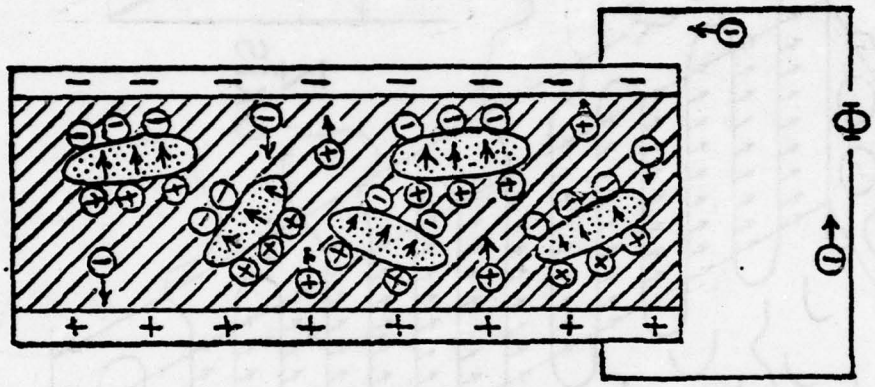

Figure 4.17 Schematic diagram of interfacial polarization in a semicrystalline polymer in an applied dc field due to charge build up at crystalline surfaces.

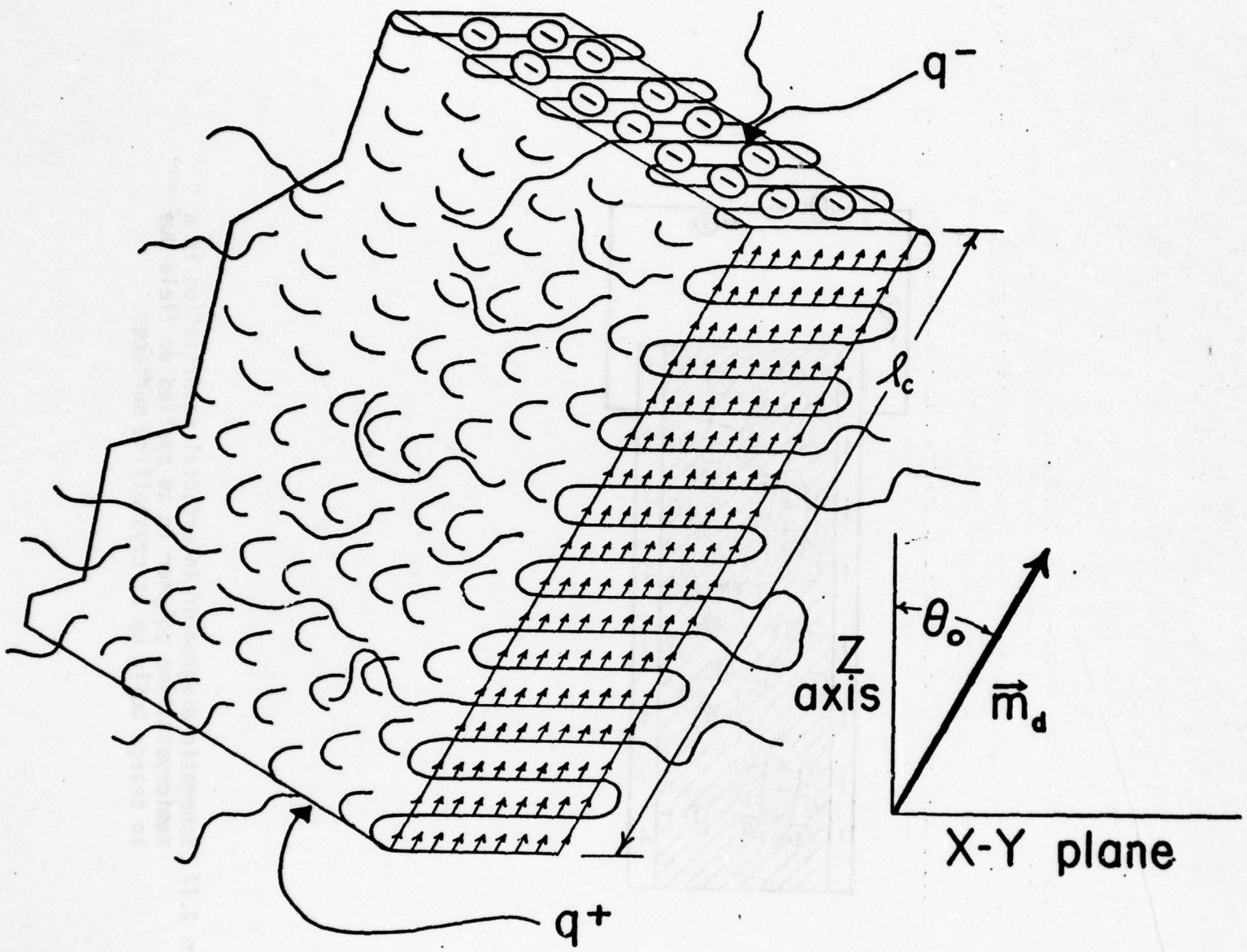

Figure 4.18 A schematic diagram illustrating dipole alignment within a polar crystal and possible counter charge at the crystal liquid interface. A typical active polymer film consists of an array of such objects with a preferential dipole alignment resulting from the poling procedure.

472:GAN:716:tam
78u472-608

TECHNICAL REPORT DISTRIBUTION LIST, CEN

	No. Copies
Office of Naval Research 800 North Quincy Street Arlington, Virginia 22217 Attn: Code 472	2
ONR Branch Office 536 S. Clark Street Chicago, Illinois 60605 Attn: Dr. George Sandoz	1
ONR Branch Office 715 Broadway New York, New York 10003 Attn: Scientific Dept.	1
ONR Branch Office 1030 East Green Street Pasadena, California 91106 Attn: Dr. R. J. Marcus	1
ONR Area Office One Hallidie Plaza, Suite 601 San Francisco, California 94102 Attn: Dr. P. A. Miller	1
ONR Branch Office Building 114, Section D 666 Summer Street Boston, Massachusetts 02210 Attn: Dr. L. H. Peebles	1
Director, Naval Research Laboratory Washington, D.C. 20390 Attn: Code 6100	1
The Assistant Secretary of the Navy (R,E&S) Department of the Navy Room 4E736, Pentagon Washington, D.C. 20350	1
Commander, Naval Air Systems Command Department of the Navy Washington, D.C. 20360 Attn: Code 310C (H. Rosenwasser)	1
Defense Documentation Center Building 5, Cameron Station Alexandria, Virginia 22314	12
U.S. Army Research Office P.O. Box 1211 Research Triangle Park, N.C. 27709 Attn: CRD-AA-IP	1
Naval Ocean Systems Center San Diego, California 92152 Attn: Mr. Joe McCartney	1
Naval Weapons Center China Lake, California 93555 Attn: Dr. A. B. Amster Chemistry Division	1
Naval Civil Engineering Laboratory Port Hueneme, California 93401 Attn: Dr. R. W. Drisko	1
Professor K. E. Woehler Department of Physics & Chemistry Naval Postgraduate School Monterey, California 93940	1
Dr. A. L. Slafkosky Scientific Advisor Commandant of the Marine Corps (Code RD-1) Washington, D.C. 20380	1
Office of Naval Research 800 N. Quincy Street Arlington, Virginia 22217 Attn: Dr. Richard S. Miller	1
Naval Ship Research and Development Center Annapolis, Maryland 21401 Attn: Dr. G. Bosmajian Applied Chemistry Division	1
Naval Ocean Systems Center San Diego, California 91232 Attn: Dr. S. Yamamoto, Marine Sciences Division	1

Encl 1

TECHNICAL REPORT DISTRIBUTION LIST, 356A

	No. Copies
Dr. Stephen H. Carr Department of Materials Science Northwestern University Evanston, Illinois 60201	1
Dr. M. Broadhurst Bulk Properties Section National Bureau of Standards U.S. Department of Commerce Washington, D.C. 20234	2
Dr. T. A. Litovitz Department of Physics Catholic University of America Washington, D.C. 20017	1
Dr. R. V. Subramanian Washington State University Department of Materials Science Pullman, Washington 99163	1
Dr. M. Shen Department of Chemical Engineering University of California Berkeley, California 94720	1
Dr. V. Stannett Department of Chemical Engineering North Carolina State University Raleigh, North Carolina 27607	1
Dr. D. R. Uhlmann Department of Metallurgy and Material Science Center for Materials Science and Engineering Massachusetts Institute of Technology Cambridge, Massachusetts 02139	1
Naval Surface Weapons Center White Oak Silver Spring, Maryland 20910 Attn: Dr. J. M. Augl Dr. B. Hartman	1
Dr. B. Goodman Globe Union Incorporated 5757 North Green Bay Avenue Milwaukee, Wisconsin 53201	1
Picatinny Arsenal SMUPA-FR-M-D Dover, New Jersey 07801 Attn: A. M. Anzalone Building 3401	1
Dr. J. K. Gillham Princeton University Department of Chemistry Princeton, New Jersey 08540	1
Douglas Aircraft Co. 3855 Lakewood Boulevard Long Beach, California 90846 Attn: Technical Library C1 290/36-84 AUTO-Sutton	1
Dr. E. Baer Department of Macromolecular Science Case Western Reserve University Cleveland, Ohio 44106	1
Dr. K. D. Pae Department of Mechanics and Materials Science Rutgers University New Brunswick, New Jersey 08903	
NASA-Lewis Research Center 21000 Brookpark Road Cleveland, Ohio 44135 Attn: Dr. T. T. Serofini, MS-49-1	1
Dr. Charles H. Sherman, Code TD 121 Naval Underwater Systems Center New London, Connecticut	
Dr. William Risen Department of Chemistry Brown University Providence, Rhode Island 02192	
Dr. Alan Gent Department of Physics University of Akron Akron, Ohio 44304	

TECHNICAL REPORT DISTRIBUTION LIST, 356A

	No. Copies
Mr. Robert W. Jones Advanced Projects Manager Hughes Aircraft Company Mail Station D 132 Culver City, California 90230	1
Dr. C. Giori IIT Research Institute 10 West 35 Street Chicago, Illinois 60616	1
Dr. M. Litt Department of Macromolecular Science Case Western Reserve University Cleveland, Ohio 44106	1
Dr. R. S. Roe Department of of Materials Science and Metallurgical Engineering University of Cincinnati Cincinnati, Ohio 45221	1
Dr. L. E. Smith U.S. Department of Commerce National Bureau of Standards Stability and Standards Washington, D.C. 20234	1
Dr. Robert E. Cohen Chemical Engineering Department Massachusetts Institute of Technology Cambridge, Massachusetts 02139	1
Dr. David Roylance Department of Materials Science and Engineering Massachusetts Institute of Technology Cambridge, Massachusetts 02039	1
Dr. T. P. Conlon, Jr., Code 3622 Sandia Laboratories Sandia Corporation Albuquerque, New Mexico	1
Dr. Martin Kaufmann, Head Materials Research Branch, Code 4542 Naval Weapons Center China Lake, California 93555	1
Dr. T. J. Reinhart, Jr., Chief Composite and Fibrous Materials Branch Nonmetallic Materials Division Department of the Air Force Air Force Materials Laboratory (AFSC) Wright-Patterson Air Force Base, Ohio 4543	1
Dr. J. Lando Department of Macromolecular Science Case Western Reserve University Cleveland, Ohio 44106	
Dr. J. White Chemical and Metallurgical Engineering University of Tennessee Knoxville, Tennessee 37916	1
Dr. J. A. Manson Materials Research Center Lehigh University Bethlehem, Pennsylvania 18015	1
Dr. R. F. Helmreich Contract RD&E Dow Chemical Co. Midland, Michigan 48640	1
Dr. R. S. Porter University of Massachusetts Department of Polymer Science and Engineering Amherst, Massachusetts 01002	1
Professor Garth Wilkes Department of Chemical Engineering Virginia Polytechnic Institute and State University Blacksburg, Virginia 24061	1
Dr. Kurt Baum Fluorochem Inc. 6233 North Irwindale Avenue Azuza, California 91702	1
Professor C. S. Paik Sung Department of Materials Sciences and Engineering Massachusetts Institute of Technology Cambridge, Massachusetts 02139	1